2009

Application of ground penetrating radar (GPR) for bridge deck condition assessment: using a 1.5 GHz ground-coupled antenna

Amos Wamweya

Department:

APPLICATION OF GROUND PENETRATING RADAR (GPR) FOR BRIDGE DECK CONDITION ASSESSMENT: USING A 1.5 GHZ GROUND-COUPLED ANTENNA

by

AMOS WAMWEYA

A THESIS

Presented to the Faculty of the Graduate School of the

MISSOURI UNIVERSITY OF SCIENCE AND TECHNOLOGY

In Partial Fulfillment of the Requirements for the Degree

MASTER OF SCIENCE IN GEOLOGICAL ENGINEERING

2009

Approved by:

Neil L. Anderson, Advisor
Mohamed G. Abdelsalam
Norbert H. Maerz

ABSTRACT

This study is a GPR-based assessment of three bridge decks, two with a hot bituminous wearing surface and one with a bare concrete slab. The primary objectives of this study were: 1) to assess the integrity of the three bridge decks using a 1.5 GHz ground-coupled GPR antenna, and 2) to evaluate the utility of the 1.5 GHz ground-coupled antenna for bridge deck investigations. Core control (chloride ion concentration data and core integrity data) and visual inspection were used as interpretive constraint.

The acquired GPR data were interpreted, and two plan view maps were generated. One depicts the magnitude of the reflections from the uppermost mat of rebar, and the second shows the arrival time of these reflections. Analysis of the GPR data and core control indicates that the magnitude of the reflected GPR signal from the uppermost mat of rebar is a direct function of concrete integrity. Higher magnitude reflections indicate higher quality concrete. To a lesser extent, the arrival time of the reflected energy is also indicative of concrete quality. Faster arrival times generally indicate higher quality concrete. Exceptions to this rule occur where the depth to the top layer of rebar varies. In this study, relative reflection amplitudes of less than 3000 on the bare concrete bridge and less than 5000 on the bituminous surface bridges indicate severe deterioration. Core control data was interpreted based on chloride ion corrosion threshold. Corrosion of rebar occurs once chloride ions content adjacent to the rebar reaches a threshold of approximately 0.033% to 0.04% by weight of concrete (or 330 ppm to400 ppm). The GPR data correlates well with the core control, indicating that the 1.5 GHz antenna is an effective tool for assessing the condition of bridge decks.

ACKNOWLEDGMENTS

I would like to thank my mother (Rita Njeri), my grandfather (Zacharia Wamwea), my Uncle (Bosco Muitherero) and the entire family for the encouragement, moral support, and financial sacrifices they have endured to see me go to school. They are mentors who have always believed in me and taught me to believe in myself. I dedicate this thesis to them.

Special thanks goes to my advisor, Dr. Neil Anderson for his support throughout my studies and giving me an opportunity to attend Missouri University of Science and Technology (MS&T) formally University of Missouri-Rolla (UMR).

I also extend my gratitude's to Dr. Mohamed Abdelsalam, Dr. Norbert H. Maerz for serving in my thesis committee. I would also like to recognize Dr. Mike Whitworth of MS&T, Dr. Robert Nusbaum, and Dr. Norman Levin both from the College of Charleston (CofC). Without them I would not have attended UMR. I greatly appreciate the effort of my fellow graduate students, Evgeniy Torgashov for helping in data acquisition and processing, and Oleg Kovin for assisting in data processing. I would like to thank Katherine Mattison the department administrative assistant and Paula Cochran the department secretary for their indefatigable desire to assist. I would like to thank Jeanine Bruening, the technical editor at MS&T writing across the curriculum program for her time in editing my thesis.

Finally, I would like to thank God for giving me the patience and the ability to finish my Masters degree.

TABLE OF CONTENTS

LIST OF ILLUSTRATIONS

LIST OF TABLES

Table Page

1. INTRODUCTION

Highways and bridges are an integral part of every successful economy in the world today. The 2007 USA National Bridge Inventory (NBI) database, which is maintained by the Federal Highway Administration (FHWA), contains 599,177 bridges built about since1904. Of all these bridges, 12% are structurally deficient and 13% are functionally obsolete. In other words, a quarter of all the bridges in the database are deficient. The main cause of deficiency in concrete bridge structures is corrosion of reinforcing steel (Sohanghpurwala, 2006). Other causes of deterioration include cracking, scaling, alkali-aggregate reaction, and spalling. Since modern economies are wholly dependent on the transportation system, a huge amount of money is spent on maintenance and repair. Transportation agencies are faced with the imperative to establish more efficient, expedient, and cost-effective methods to assess subsurface conditions of bridge decks. The key to cutting costs and increasing the service life of a bridge deck is the ability to diagnose problems at an early stage. Such diagnoses are difficult, however, since most deteriorations (e.g., corrosion) are internal and take years to manifest on the surface of the structure. Traditional deck inspection methods include sounding (hammer or chain dragging), impact-echo, ultrasonic pulse velocity, and infrared thermography. Of all the technologies developed thus far, GPR is the most promising, expedient, and reliable nondestructive technology (NDT) for bridge deck assessment.

The GPR tool operates by transmitting a short pulse of electromagnetic (EM) energy into the surface and recording reflections at interfaces of materials with different dielectric properties. The GPR data includes four main components: a) changes in

reflection strength, b) changes in arrival times of specific reflections, c) source wavelet distortion, and d) signal attenuation (Cardimona *et al.*, 2001). When applied to bridge deck assessment, these GPR signatures can detect corrosion of steel reinforcement within the concrete deck, which can be an indicator of poor quality overlay bonding or delamination at the rebar level (Cardimona *et al.*, 2001). Since EM energy is very sensitive to metals, diffractions from the rebar in concrete bridge decks can be clearly seen as hyperbolic images on the GPR data. An intact rebar has a very high reflection amplitude and a clear hyperbolic shape, whereas corroded rebar leads to significant attenuation of the reflected GPR signal and hence a blurred image. Depending on the level of deterioration, there may be no visible reflection at all. Corrosion and delamination may also be apparent in the late arrival times of signal reflection. Such delays are the result or reduced signal velocity, which makes the affected rebar appear deeper than the intact rebar. However, in this study, estimation of deterioration based on rebar depth was impossible due to varying rebar placement depths (which was the result of design flaws).

Reflection amplitudes are site-specific and can vary even within the same bridge deck depending on the concrete admixtures. Therefore, estimation of deterioration based on the magnitude of reflections maybe inaccurate. Chloride ion concentration analysis was used to validate the GPR data. Relative amplitudes of <3000 on the concrete slab and <5000 on asphalt ovelayed bridges were interpreted as indicative of significant deterioration and high chloride ion content (above 400ppm). Areas of relative amplitudes of >3000 <4500 on the concrete slab and >5000 <7000 on asphalt ovelayed bridges were interpreted to indicate mild deterioration and elevated chloride ion content.

Of all bridge deck evaluations carried out using GPR, the most accurate have used the high frequency (1.5 GHz) ground-coupled antenna (GSSI MN 43-7 Rev C, 2007). The GSSI 1.5 GHz ground-coupled antenna was specifically designed for bridge deck assessment; it offers rapid data acquisition and yields high resolution data (increased details) compared to traditional NDT such as chain dragging. The 1.5 GHz antenna has a penetration depth of approximately 18 inches in concrete, which is more than adequate for accurate location of the top rebar layer (GSSI MN 43-7 Rev C, 2007).

Experimentation is currently underway to improve the air-launched antennas which in the future may replace the ground-coupled antennas for bridge deck assessment. The GSSI high frequency 2GHz air-launched horn antenna offers a vehicle-mounted solution with rapid, safe data acquisition methodology; however, it cannot match the resolution offered by the 1.5GHz ground-coupled antenna. This development illustrates the intensive approach that GPR technology developers are taking to improve this tool and make it more users friendly.

1.1. BRIDGE DECKS DESCRIPTION

This case study assessed three separate bridge decks, Bridge A-090-0095, and Bridge C-(048-0011 and 048-0012) are asphalt covered concrete. Bridge B-90-0087 is concrete only. This study began with a visual inspection of each structure to evaluate the level of visible deterioration. These inspections permitted an evaluation of the effectiveness of the GPR tool for assessing minor to severe problems. Below is a short description of each bridge deck.

1.1.1. Concrete Bridge A-090-0095. Constructed in 1971, this bridge is rated in the NBI as structurally deficient. It is approximately 286 feet long with single lane in both the westbound and eastbound directions. Both lanes are approximately 23 feet wide with a hot bituminous wearing surface and separated by an 18 ft wide concrete median. At the time of inspection the asphalt on the southern edge (close to the median) of the westbound lane (Figure 1.1) was severely deteriorated with numerous potholes, patches, seals, and substantial accumulated debris. The eastbound lane was in fair condition (visually) with few patches and seals, but it had accumulated mud on the southern shoulder (Figure 1.2).

Figure 1.1. Severely deteriorated section of westbound lanes on Bridge A-090-0095.

Figure 1.2. Accumulated mud at the southern shoulder of Bridge A-090-0095 eastbound.

1.1.2. Concrete Bridge B-90-0087. Built in 1932 and reconstructed in 1979, the deck is a reinforced structural concrete slab measuring approximately 176 feet long by 24 feet wide and carrying both the north- and southbound traffic. The NBI classifies this bridge as structurally deficient and indicates that it is a high priority for replacement. The bridge visual inspection showed significant transverse cracking, numerous small patches, and some scaling (Figure 1.3).

Figure 1.3. Concrete mortar removal and numerous small patches on concrete Bridge B-090-0087.

1.1.3. Bridge C-(048-0011 and 048-0012). This is a concrete bridge structure with a hot bituminous wearing surface. The bridge was built in 1963, and according to NBI it is in good condition (Figure 1.4). Both the westbound (Bridge C-048-0011) and eastbound directions (Bridge C-048-0012) have double lanes approximately 109 feet long by 26 feet wide. The surface of all lanes was in good condition apart from a few small patches along the end expansion joints. However, the underside of the westbound lanes had severe corrosion that had led to debonding of the concrete and exposure of the bottom rebar mat (Figure 1.5).

Figure 1.4. Bridge C-(048-0011 and 048-0012) with Bridge C-048-0012 in the foreground and C-048-0011 in the background.

Figure 1.5. Underside of Bridge C- 048-0011 (westbound) showing corrosion deterioration and debonding of concrete at rebar level.

2. BRIDGE DECKS

2.1. OVERVIEW

High strength and durability are important aspects in bridge deck design (Jestings & Sen, 2003), the primary materials used in modern bridge structures are concrete and steel. With constant use and exposure to the environment, however, even these high strength, durable materials are subject to wear and tear, limiting their service life. Highways and bridges are an integral part of every successful economy in the world today. A good transportation system should allow reasonable travel speed and ensure safety for both people and cargo (Morse and Green, 2003). Since modern economies are wholly dependent on the transportation system, bridge closures for repair and maintenance are costly. Therefore pavement should be designed to last as long as possible with minimal maintenance.

Not until the 1967 collapse of the Silver Bridge in Point Pleasant did the FHWA develop the guidelines requiring the inspection of every public bridge at least once every two years (Yehia *et al.*, 2007). The 2007 United States NBI database which is maintained by the FHWA contains 599,177 bridges (Table 2.1) built since about 1904. Of all these bridges, 12% (72,178) are structurally deficient (Table, 2.2), and 13% (79,635) are functionally obsolete (Table, 2.3). In other words a quarter of those recorded bridges are deficient. Bridges are considered structurally deficient if significant load carrying elements are found to be in poor condition due to deterioration, or if the waterway opening is extremely insufficient, causing intolerable traffic interruptions (Iowa DOT website). Functionally obsolete bridges are not automatically rated as structurally deficient, nor are they inherently unsafe, but they do not meet today bridge building

standards. Such bridges may have lane widths, shoulder widths, or vertical clearances inadequate for current traffic demand, or they may be subject to occasional flooding (Iowa DOT website). A map on the American Traffic Safety Service Association website (ATSSA) (Figure 2.1) shows the distribution of structurally deficient bridge within the United States.

The cost to maintain the nation's bridges during the 20 years period from 1999 to 2019 is estimated to be $5.8 billion per year, and the cost to improve and eliminate deficiency over the same period is $10.6 billion (Sohanghpurwala, 2006). Condition rating in 2002 NBI showed that 14 percent of the structurally deficient bridges were subject to corrosion of reinforced steel (Sohanghpurwala, 2006). A 2001 study of corrosion in the industrial sector broadly was carried out by an interdisciplinary team. This study estimated that 16% (40.16 billion) of the total $276 billion direct cost of corrosion went to infrastructure, with $8.3 billion going to highway bridges alone. The indirect cost was estimated to equal the direct cost. (Roberge, 2007).

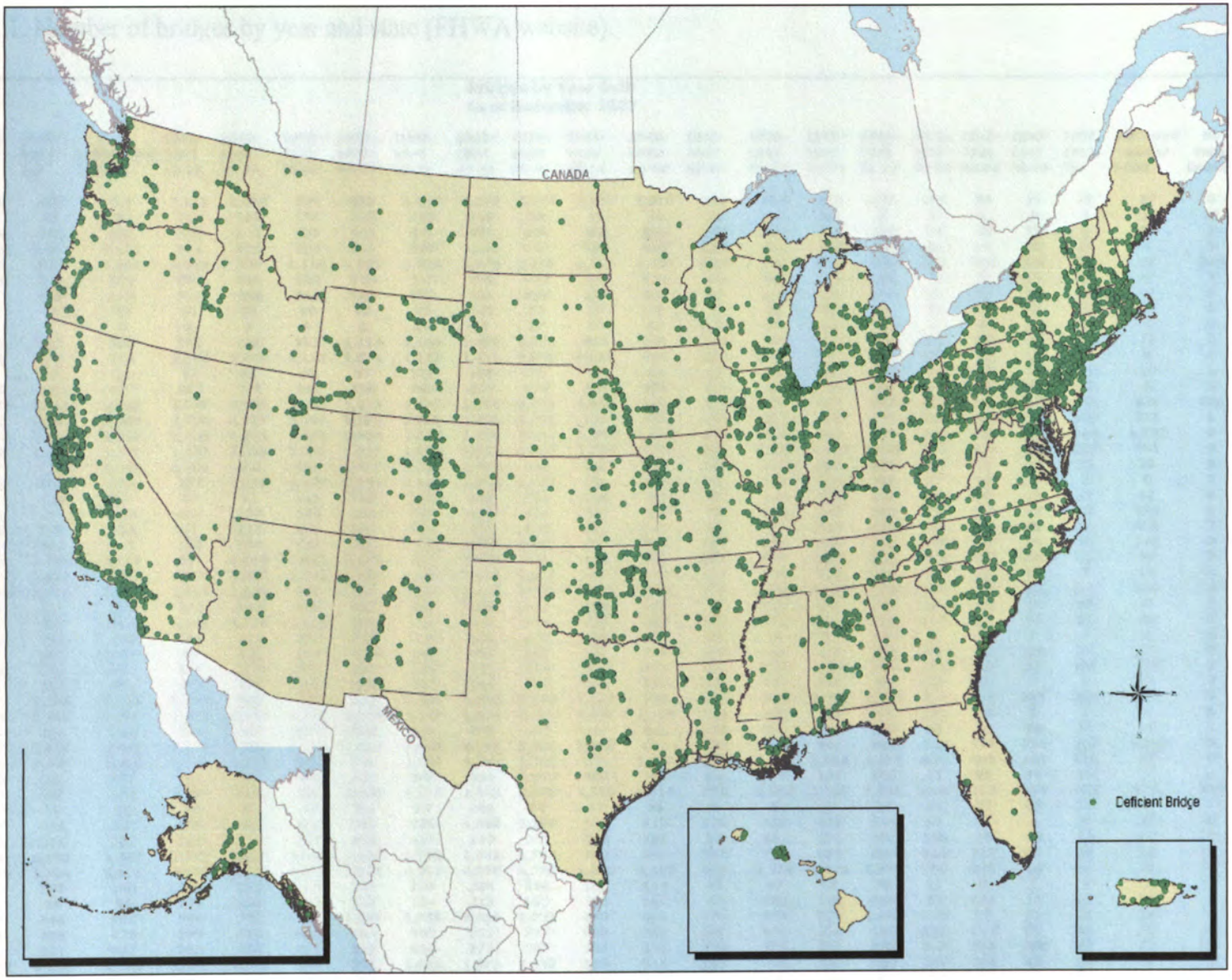

Figure 2.1. Location map of structurally deficient bridges in United States (ATSSA Website).

Table 2.1. Number of bridges by year and state (FHWA website).

Bridges by Year Built
As of December 2007

Yr Built / Age	2003-2007 0-4	1998-2002 5-9	1993-1997 10-14	1988-1992 15-19	1983-1987 20-24	1978-1982 25-29	1973-1977 30-34	1968-1972 35-39	1963-1967 40-44	1958-1962 45-49	1953-1957 50-54	1948-1952 55-59	1943-1947 60-64	1938-1942 65-69	1933-1937 70-74	1928-1932 75-79	1923-1927 80-84	1918-1922 85-89	1913-1917 90-94	1907-1912 95-	1904 and earlier >100	No Value Coded
AL	776	868	956	1,178	1,083	764	913	1,222	1,518	1,574	1,257	1,018	320	834	516	547	307	84	35	22	87	0
AK	86	89	99	119	157	155	135	100	108	52	41	30	11	10	11	0	0	1	0	2	6	17
AZ	333	406	397	714	573	516	448	671	899	669	381	248	107	282	301	289	34	37	19	6	55	1
AR	795	1,002	1,011	894	924	872	961	995	1,126	762	588	649	136	505	358	783	98	46	10	12	1	5
CA	356	833	1,064	1,225	875	1,114	1,899	3,395	3,778	2,680	1,619	1,321	407	799	582	788	486	318	220	99	53	266
CO	358	674	822	974	846	530	509	637	796	655	313	321	61	256	346	160	55	23	14	14	5	2
CT	47	122	125	349	250	196	163	333	631	599	327	142	59	219	194	137	60	45	28	44	97	0
DE	26	51	73	86	55	56	78	90	101	62	25	28	2	20	24	21	12	21	6	3	16	0
DC	2	2	0	0	1	0	2	26	61	37	30	15	10	22	14	8	1	0	3	6	4	0
FL	573	907	869	969	788	793	1,114	1,188	1,489	1,220	657	496	114	198	77	73	98	17	5	2	17	0
GA	506	643	992	1,177	1,119	1,113	1,078	1,173	1,474	1,685	1,003	886	203	517	391	349	132	79	17	12	8	0
HI	7	17	24	23	41	60	97	127	130	70	69	61	22	54	85	77	54	35	17	29	15	2
ID	128	181	167	254	229	285	504	487	539	459	305	151	28	87	114	101	27	24	17	13	0	4
1L	1,038	1,616	2,085	2,268	2,563	2,480	1,837	1,798	1,958	2,211	1,098	528	182	566	577	727	412	292	193	541	801	186
IN	668	1,186	1,345	1,620	1,557	1,189	1,553	1,682	1,715	1,348	707	435	160	537	513	746	364	432	154	208	298	1
IA	1,272	1,543	1,353	1,488	1,684	1,675	1,936	1,860	1,794	1,942	1,818	1,616	380	904	466	494	451	423	383	144	1,117	0
KS	749	1,320	1,422	1,353	1,598	1,586	1,533	1,622	1,823	1,996	1,793	1,179	569	1,324	1,448	1,949	472	620	175	397	501	0
KY	317	729	1,009	1,316	902	851	1,053	1,288	1,082	905	825	950	160	509	681	661	261	79	15	13	29	0
LA	488	755	879	977	1,337	1,177	1,381	1,502	1,520	1,423	755	492	74	142	135	251	37	10	2	3	0	2
ME	86	109	82	87	91	111	117	111	208	204	279	179	67	137	178	168	76	55	13	11	17	0
MD	129	231	288	466	309	306	426	477	511	423	328	232	74	103	145	240	79	108	44	59	138	9
MA	140	190	139	91	123	179	169	248	553	576	749	273	55	363	195	166	102	87	64	96	426	2
MI	453	614	555	594	754	739	795	1,195	1,070	1,292	487	310	142	304	330	510	278	192	54	86	148	0
MN	793	1,154	1,029	982	1,040	1,622	1,030	953	1,076	705	513	331	107	407	260	309	244	177	190	70	58	6
MS	1,121	1,697	1,923	1,501	1,437	1,305	1,433	1,367	1,516	1,421	645	574	111	408	317	132	39	25	11	4	15	0
MO	1,600	2,331	2,090	1,855	1,094	855	924	1,159	1,427	1,759	1,206	1,065	316	909	1,021	1,719	634	699	120	345	900	2
MT	136	194	191	222	357	414	436	541	526	483	259	252	77	289	247	175	34	39	44	43	17	3
NE	752	990	999	1,267	1,276	1,026	908	799	918	818	429	458	127	381	3,681	214	106	92	89	98	20	0
NV	116	282	225	134	116	60	145	126	221	111	48	27	21	18	27	16	3	4	0	1	3	0
NH	63	102	86	90	125	133	137	164	207	250	136	118	38	155	148	189	51	60	10	19	76	0
NJ	149	248	302	276	279	220	429	732	536	386	570	471	81	248	216	392	231	138	92	105	304	2
NM	88	183	158	173	235	306	376	467	442	320	221	186	65	293	224	86	12	5	2	5	0	3
NY	591	1,008	1,053	1,173	783	789	872	1,431	1,500	1,440	1,371	760	255	853	1,020	1,104	307	178	175	284	366	0
NC	904	1,286	1,399	1,275	1,071	1,273	1,239	1,467	1,636	2,196	1,587	1,200	124	320	186	195	192	209	5	6	4	9
ND	139	200	208	254	297	373	349	380	402	400	257	291	117	211	207	139	48	82	54	34	11	1
OH	1,228	1,944	2,145	2,074	1,582	1,222	1,658	2,700	2,599	2,356	1,810	872	355	854	601	902	326	277	232	222	1,980	0
OK	923	1,624	1,556	1,710	1,373	965	945	1,186	1,343	1,388	975	1,547	583	3,451	1,408	1,374	502	400	104	125	17	0
OR	389	343	323	323	445	568	568	665	950	1,040	650	286	81	137	126	160	95	96	41	23	5	2
PA	512	937	823	1,090	966	509	1,250	1,575	1,845	1,905	1,382	1,315	288	1,553	1,307	1,486	815	719	464	504	912	64
RI	4	12	36	26	23	13	30	95	161	84	37	31	8	9	21	38	24	22	16	12	44	1
SC	346	570	693	466	455	540	781	928	1,065	1,194	583	418	110	403	178	304	99	41	4	4	39	0
SD	293	328	281	332	270	273	408	427	570	503	354	281	96	361	373	409	136	79	38	73	33	0
TN	714	1,202	1,457	1,498	3,016	1,045	1,288	1,762	1,662	1,792	762	987	257	777	424	676	335	107	45	13	16	0
TX	2,774	3,234	3,059	4,135	3,480	2,627	2,898	4,267	4,576	4,750	3,499	2,533	908	2,318	1,999	1,972	799	308	48	41	41	1
UT	143	302	149	201	305	173	232	305	334	245	106	114	47	47	67	39	21	9	7	2	0	2
VT	50	98	95	105	122	134	223	184	213	193	104	106	42	243	150	269	83	162	16	16	95	6
VA	485	745	853	949	783	963	1,166	1,356	1,519	1,039	533	436	178	363	303	1,402	170	67	51	21	33	2
WA	285	369	478	366	410	465	583	840	921	777	620	451	147	164	200	196	120	112	85	39	56	0
WV	310	622	667	786	469	493	498	424	372	307	194	288	102	223	201	255	247	208	184	73	77	0
WI	1,003	1,120	1,195	1,350	1,130	908	986	1,033	1,071	1,036	506	516	105	404	323	485	241	203	88	54	35	1
WY	75	125	142	173	225	207	271	355	419	511	190	127	20	45	48	45	18	15	11	6	0	2
PR	86	138	223	146	83	155	210	273	147	122	83	112	43	106	30	27	61	41	13	6	37	0
Totals	25,405	37,476	39,594	43,154	41,106	36,383	40,974	50,188	55,058	52,375	35,084	27,713	8,152	24,642	22,994	23,954	9,889	7,602	3,727	4,070	9,033	604

Total Bridges 599,177

Table 2.2. Structurally deficient bridges by year and state (FHWA website).

Structurally Deficient Bridges by Year Built
As of December 2007

Yr Built / Age	2003-2007 0-4	1998-2002 5-9	1993-1997 10-14	1988-1992 15-19	1983-1987 20-24	1978-1982 25-29	1973-1977 30-34	1968-1972 35-39	1963-1967 40-44	1958-1962 45-49	1953-1957 50-54	1948-1952 55-59	1943-1947 60-64	1938-1942 65-69	1933-1937 70-74	1928-1932 75-79	1923-1927 80-84	1918-1922 85-89	1913-1917 90-94	1907-1912 95-	1904 and earlier >100	No Value Coded
AL	0	0	26	46	45	54	100	125	155	206	179	207	79	217	190	121	60	36	16	13	23	0
AK	0	0	3	8	17	29	15	12	21	12	10	15	4	2	1	0	0	1	0	0	3	2
AZ	0	0	3	0	6	10	13	17	18	27	16	12	3	6	18	19	3	2	5	0	6	0
AR	0	0	27	75	61	43	92	133	97	88	61	70	23	79	32	60	18	21	7	7	1	1
CA	0	0	46	100	83	101	214	459	593	401	230	173	77	129	90	166	75	61	57	23	17	40
CO	0	0	3	3	19	25	23	34	95	78	40	46	11	67	67	40	10	11	3	4	1	0
CT	0	0	3	8	9	7	5	24	34	44	35	20	6	33	32	34	11	13	3	14	20	0
DE	0	0	0	0	3	2	0	1	1	2	0	4	0	0	1	1	0	0	1	1	3	0
DC	0	0	0	0	0	0	0	1	5	1	4	5	0	5	0	0	0	0	0	1	2	0
FL	0	0	6	7	17	13	13	36	37	57	33	28	10	22	2	10	8	2	0	1	0	0
GA	0	0	7	22	38	48	55	60	75	168	140	172	36	71	38	46	19	19	3	5	4	0
HI	0	0	1	0	1	0	8	8	9	0	1	7	3	9	10	28	15	10	9	16	7	0
ID	0	0	0	5	5	12	22	28	47	50	30	24	4	17	45	29	6	10	8	6	0	1
IL	0	0	4	8	27	63	101	120	217	278	186	97	27	112	126	198	128	106	90	266	312	16
IN	0	0	10	19	39	63	83	144	197	135	73	86	29	150	127	250	125	157	70	95	138	0
IA	0	0	9	15	33	91	170	211	309	585	723	689	173	433	186	189	175	215	209	103	611	0
KS	0	0	3	8	12	28	56	106	142	203	160	226	134	297	219	447	115	281	81	283	166	0
KY	0	0	6	32	61	61	81	108	144	163	71	112	23	105	120	133	63	38	11	9	17	0
LA	0	0	14	43	78	121	170	273	289	307	152	128	24	61	35	71	6	4	2	2	0	0
ME	0	0	3	6	7	5	5	10	11	18	54	33	11	28	56	49	23	14	4	2	10	0
MD	0	0	4	3	4	8	14	26	38	45	29	37	10	19	25	30	19	29	6	14	26	0
MA	0	0	1	1	3	7	5	12	55	50	57	31	10	71	45	54	26	29	14	21	82	0
MI	0	0	4	8	13	35	74	179	152	184	94	65	25	94	95	167	107	95	36	55	87	0
MN	0	0	2	1	5	12	41	61	126	121	119	77	25	93	60	64	81	82	118	32	26	3
MS	0	0	178	226	173	185	319	337	357	368	217	185	38	164	133	72	16	10	9	2	8	0
MO	0	0	29	37	37	70	120	137	207	378	326	368	117	363	430	654	205	326	67	190	356	0
MT	0	0	5	8	29	32	23	33	40	31	26	34	9	44	34	38	11	14	26	26	8	1
NE	0	0	3	5	14	20	42	60	58	75	64	85	22	64	1,574	54	31	54	55	63	14	0
NV	0	0	2	0	2	0	5	2	7	2	4	4	3	5	5	1	1	2	0	0	1	0
NH	0	0	0	4	9	14	15	16	14	33	19	30	9	51	29	55	5	23	5	6	43	0
NJ	0	0	0	1	5	2	10	28	32	48	35	49	21	55	49	109	74	50	21	40	106	1
NM	0	0	1	3	6	23	42	63	53	48	39	20	4	40	25	28	6	1	1	0	0	1
NY	0	0	5	19	31	61	77	110	143	200	191	114	51	204	239	295	82	52	46	83	115	0
NC	0	0	8	12	24	41	126	202	364	439	410	349	33	76	29	45	56	49	3	4	2	0
ND	0	0	2	3	2	10	12	40	37	45	55	88	47	88	98	65	26	47	38	29	9	0
OH	0	0	5	18	26	59	102	249	200	280	233	169	62	179	145	215	106	76	71	67	580	0
OK	0	0	106	148	121	107	143	273	248	336	227	703	218	1,394	451	611	220	248	87	110	15	0
OR	0	0	2	7	6	11	13	37	60	117	86	39	20	22	25	25	14	14	13	3	0	0
PA	0	0	12	28	39	51	131	270	300	428	367	347	103	582	574	707	445	366	241	278	463	25
RI	0	0	0	1	1	2	5	14	24	34	14	13	4	4	6	8	4	5	8	6	10	0
SC	0	0	14	27	12	36	80	104	162	272	188	99	26	116	35	53	20	8	1	1	6	0
SD	0	0	0	11	15	26	39	48	73	80	53	80	36	151	168	193	71	58	29	64	16	0
TN	0	0	16	28	36	51	139	175	164	174	73	105	28	105	60	71	48	26	12	5	7	0
TX	0	0	60	120	157	108	73	146	133	209	149	194	76	238	149	170	51	78	14	24	36	0
UT	0	0	3	2	10	9	11	20	57	17	7	22	21	13	16	7	6	5	2	2	0	2
VT	0	0	0	4	2	4	15	18	28	31	23	17	14	61	40	83	32	56	7	11	54	0
VA	0	0	12	10	14	35	59	78	113	119	58	71	29	76	60	331	63	24	25	14	16	0
WA	0	0	1	0	3	16	14	27	38	46	38	43	15	18	38	37	18	19	13	8	8	0
WV	0	0	1	20	20	47	53	48	72	80	75	96	25	59	52	76	75	83	82	39	50	0
WI	0	0	2	6	6	16	48	103	109	139	97	117	29	127	89	168	74	76	49	29	14	0
WY	0	0	7	13	18	37	33	50	42	48	19	26	8	17	18	29	7	8	6	3	0	0
PR	0	0	8	6	6	6	19	35	18	18	12	15	10	11	12	7	22	12	4	3	15	0
Totals	0	0	667	1,185	1,410	1,917	3,128	4,911	6,020	7,318	5,602	5,846	1,825	6,447	6,203	6,413	2,882	3,026	1,688	2,083	3,514	93
TOTALS 12%			72,178																			

Table 2.3. Number of functionally obsolete bridges by year and state (FHWA website).

Functionally Obsolete Bridges by Year Built
As of December 2007

Yr Built	2003-2007	1998-2002	1993-1997	1988-1992	1983-1987	1978-1982	1973-1977	1968-1972	1963-1967	1958-1962	1953-1957	1948-1952	1943-1947	1938-1942	1933-1937	1928-1932	1923-1927	1918-1922	1913-1917	1907-1912	1904 and earlier	No Value
Age	0-4	5-9	10-14	15-19	20-24	25-29	30-34	35-39	40-44	45-49	50-54	55-59	60-64	65-69	70-74	75-79	80-84	85-89	90-94	95-100	>100	Coded
AL	0	0	44	67	64	63	74	132	258	301	300	212	90	246	94	107	67	17	7	4	11	0
AK	0	0	22	27	19	32	20	8	2	9	9	6	1	4	7	0	0	0	0	0	1	12
AZ	0	0	35	66	40	31	36	29	135	77	26	10	4	22	29	23	12	8	9	3	13	0
AR	0	0	134	121	118	93	93	109	190	146	141	201	26	163	147	184	29	9	1	3	0	1
CA	0	0	144	119	88	87	202	349	539	512	400	303	115	227	173	197	126	93	53	38	18	51
CO	0	0	47	72	77	26	53	75	130	118	49	44	3	20	48	38	15	4	4	3	0	0
CT	0	0	19	82	45	24	31	48	147	180	80	39	26	83	83	44	16	14	13	17	47	0
DE	0	0	2	7	5	2	10	3	30	6	4	2	1	6	6	10	5	5	2	0	6	0
DC	0	0	0	0	0	0	2	17	27	21	18	6	6	8	7	6	1	0	1	5	2	0
FL	0	0	78	74	76	72	151	170	326	331	144	102	27	45	12	30	45	5	4	1	0	0
GA	0	0	63	62	67	63	59	98	287	324	231	239	65	107	75	71	30	28	10	4	1	0
HI	0	0	1	2	8	8	10	21	36	34	26	24	11	22	52	33	33	16	7	9	4	0
ID	0	0	7	18	20	18	37	67	86	79	30	20	2	13	22	17	3	6	5	1	0	1
1L	0	0	87	62	60	52	64	111	202	339	131	86	11	44	58	78	63	71	50	81	142	35
IN	0	0	83	104	84	86	137	165	240	195	149	75	26	98	86	127	66	84	46	48	85	0
IA	0	0	44	22	37	61	62	69	134	142	118	157	44	95	52	75	68	66	50	14	139	0
KS	0	0	58	52	47	85	106	139	183	219	311	130	97	144	170	267	116	124	33	44	40	0
KY	0	0	132	236	155	165	271	289	218	164	160	223	49	178	250	277	120	29	2	2	8	0
LA	0	0	90	95	100	87	147	301	392	381	272	152	11	35	44	65	7	1	0	0	0	0
ME	0	0	8	9	16	17	10	16	17	51	82	51	17	39	58	33	20	16	3	4	1	0
MD	0	0	43	60	43	51	51	59	89	91	64	40	18	29	44	115	32	44	23	27	56	1
MA	0	0	54	34	44	95	76	103	291	193	396	104	21	86	70	49	44	38	26	44	202	1
MI	0	0	40	50	64	45	83	148	176	236	105	58	21	31	43	76	52	44	6	9	15	0
MN	0	0	11	19	11	19	9	47	79	55	15	9	5	21	19	13	30	15	19	18	6	0
MS	0	0	60	44	35	46	42	56	267	333	92	114	23	67	84	25	14	4	2	1	6	0
MO	0	0	264	230	137	129	95	156	246	319	197	185	40	152	161	347	137	137	12	39	119	1
MT	0	0	8	10	38	37	49	58	88	76	30	22	11	30	36	18	5	7	7	10	2	0
NE	0	0	10	20	43	38	36	79	69	59	45	56	11	33	625	26	30	19	15	23	3	0
NV	0	0	10	9	10	3	10	31	37	30	5	0	1	2	5	2	0	0	0	0	1	0
NH	0	0	10	8	12	16	13	10	33	30	32	25	13	28	37	41	16	12	3	6	10	0
NJ	0	0	40	18	38	34	131	238	161	67	191	120	25	57	47	79	66	31	33	27	83	1
NM	0	0	12	11	21	22	30	45	45	29	22	4	5	26	11	7	1	1	0	2	0	0
NY	0	0	169	224	107	117	127	447	575	525	523	246	68	244	303	315	95	76	76	125	136	0
NC	0	0	74	88	83	51	91	138	382	628	534	331	29	86	68	44	67	88	0	2	0	3
ND	0	0	5	2	6	13	19	17	24	17	14	25	9	22	23	15	10	14	8	4	0	1
OH	0	0	189	175	139	135	228	469	501	365	381	171	70	166	128	201	62	66	53	50	440	0
OK	0	0	45	76	49	38	99	133	184	172	115	124	34	223	76	120	75	38	7	6	0	0
OR	0	0	30	27	44	59	57	54	163	225	144	71	26	44	35	68	38	38	15	15	0	0
PA	0	0	102	186	198	57	169	238	304	338	305	293	34	283	224	308	194	169	122	115	242	20
RI	0	0	16	10	8	4	6	30	61	20	4	8	1	3	7	12	10	7	5	3	17	0
SC	0	0	24	42	27	28	40	76	103	185	63	50	13	48	26	48	21	4	2	3	5	0
SD	0	0	10	9	7	8	7	14	39	37	17	15	8	15	19	33	9	3	2	5	4	0
TN	0	0	70	96	174	116	137	215	318	368	155	273	66	294	150	188	98	38	16	2	2	0
TX	0	0	530	864	709	449	504	544	850	991	632	595	142	350	235	260	99	69	17	6	2	0
UT	0	0	8	11	31	7	19	28	58	35	10	16	4	5	14	5	3	0	0	0	0	0
VT	0	0	11	6	9	22	28	35	41	33	9	20	11	55	47	62	17	37	3	2	17	1
VA	0	0	105	81	60	72	128	131	251	236	153	159	61	128	104	458	55	23	19	3	7	0
WA	0	0	68	79	61	56	77	120	224	224	202	141	44	57	77	79	61.	49	23	11	13	0
WV	0	0	128	220	110	124	110	73	73	69	36	66	25	68	65	81	105	75	58	13	17	0
WI	0	0	53	38	37	28	45	49	120	104	36	52	10	39	30	59	40	23	15	6	4	1
WY	0	0	5	5	8	5	27	14	55	66	9	10	2	3	6	6	6	1	2	1	0	0
PR	0	0	54	50	36	66	66	76	77	58	45	74	22	76	16	18	34	23	8	2	20	0
Totals	0	0	3,356	4,099	3,525	3,062	4,184	6,147	9,563	9,843	7,262	5,559	1,505	4,370	4,308	4,860	2,368	1,789	897	861	1,947	130
	TOTALS 13%		79,635																			

With corrosion of steel becoming an expensive and persistent problem, civil engineers at Purdue University are developing a new generation of bridge decks with fiber-reinforced polymers (FRP) in place of top steel rebar reinforcement mat. Professor of civil engineering Robert Frosch, stated that replacing the bridge deck rebar mat with polymers will extend the lifetime of a deck to perhaps 50 to 100 years while increasing the number of years between expensive repairs (Perdue University news website, 2005). The FRP is not subject to electrochemical corrosion, it has the potential to revolutionalize the way bridge decks are built by replacing steel in the top rebar mat. However, FRPs have some disadvantages (Table 2.4) that that need to be addressed before their full implementation.

Table 2.4. Summary of the advantages and disadvantages of FRPs (FHWA, 2006).

ADVANTAGES	DISADVANTAGES
• High longitudinal strength. • Nonmagnetic. • Corrosion resistance. • High fatigue endurance. • Light weight (about one-fifth to one-fourth the density of steel). • Low thermal and electric conductivity.	• High cost. • No yielding before brittle rupture. • Low transverse strength. • Low modulus of elasticity. • Susceptibility to damage due to ultra-violet radiation. • Low durability of glass fibers in a moist environment. • Low durability of some glass and aramid fibers in an alkaline environment. • High CTE perpendicular to the fibers, relative to concrete. • Susceptibility to fire, depending on matrix type and concrete cover.

2.2. BRIDGE DECK DETERIORATION

Bridge integrity is undermined by delamination of concrete and corrosion of embedded steel reinforcement. Delamination is the separation of concrete in planes and decoupling of the concrete from rebar. It is generally the results of tensile failure (Sohanghpurwala, 2006; Kim, 2003). State departments of transportation (DOTs) indicate that the extent of concrete delamination that requires action is between 5% and 20% of the total deck area (Guthrie and Hema, 2005). Bridges may also deterioration prematurely due to inferior materials, poor workmanship, or inadequate design. Overtime concrete becomes more porous for a variety of reasons, including loading temperature stresses, vibration, and frequent alternation of freezing and thawing. With time, the pores, fissures, capillaries, crevices, and cracks open and enlarge, and deterioration process is accelerated by water, debris, and the build-up of chemicals from de-icing salt. Bridge decks are subject not only to corrosion, but also to alkali-aggregate reaction, cracking, scaling, and spalling, all of which are interdependent. Table 2.5 summarizes causes of bridge decks deterioration.

Table 2.5. Summary of common problems in concrete bridge decks (Yehia *et al.*, 2007)

Defect	Definition	Cause
Spalling	Concrete falls away leaving a little hole that defines the fracture surface	Internal pressure due to freezing and thawing, insufficient consolidation during construction and the formation of inner cracks which are later transformed to spalls
Corrosion of reinforcement	Weakening of some metals such as steel due to exposure to corrosive environment where it becomes brittle and goes back to its ore state	Presence of a conductive solution, corrosion agent, and a corrosion cell
Leaching	Drainage or removal of soluble or constitutes in porous materials by water seeping action	Occurs due to dissolving water constitutes like calcium hydroxide at crack locations
Scaling	Deterioration of concrete into smaller parts and individual aggregates	Scaling may be a result of freezing and thawing, and chemical attacks
Cracking	Breakage in the concrete causing a discontinuity without causing a complete separation of the structure	Cracks form due to tensile forces caused by shrinkage, temperature changes, bending, loading, corrosion of reinforcement, sulfates, and chemical attacks
Honeycombing	The presence of exposed coarse aggregate without enough concrete paste covering the aggregates, causing the presence of small holes	Poorly graded concrete mix, the use of large coarse aggregates, and insufficient vibration at the time of placement
Delaminations	Cracks or fracture planes at or just above the level of reinforcement that grow big and can affect the integrity of the structure	Corrosion of steel reinforcement, high amount of moisture and chloride content, and the presence of cracks in concrete surface

2.2.1. Corrosion. This is a costly and severe material science problem (Sastri, 1998), that has challenged engineers since the earliest use of metals. In recent years, corrosion mitigation has received increased attention due to widespread occurrence and the high cost of repair. Corrosion occurs by chemical or electrochemical processes (Brown *et al.*, 1979). On most bridges electrochemical processes are the prevalent mode of corrosion. The electrochemical process requires an anode (where corrosion occurs), a cathode (maintains ionic balance) and an electrolyte (which functions as a charge transport medium) (Brown *et al*, 1979). These components combine to form an electrochemical cell where oxidation leads to rust.

Oxygen and moisture converts iron into iron oxide, thus corroding the steel rebar. Chloride ions induce and sustain corrosion. Cracking and scaling increase the rate of corrosion by harboring the required elements (water, oxygen, salts). Chloride induced corrosion occurs once chloride ions adjacent to the rebar reaches a threshold value of approximately 0.025% to 0.033% by weight of concrete (Sohanghpurwala, 2006).

Aqueous corrosion of iron in the presence of oxygen occurs through two partial reactions, one anodic and the other cathodic. Equations (1) and (2) express these reactions. Since Iron is very high in the electromotive-force series, it has a strong tendency to enter into solution (Fromm *et al.*, 1979), thereby liberating electrons at the anode (equation 1).

$$Fe_{metal} \rightarrow Fe^{++}_{hydrated} + 2e^{-} \text{ (Oxidation reaction)} \quad (1)$$

In order to maintain equilibrium (charge neutrality), electrons liberated by the anodic reaction are consumed at the cathodic reaction, which depends on the pH and the amount of dissolved oxygen (equation 2). The potential (E), at which the sum of the anodic and cathodic reaction rates equals zero, is labeled the corrosion potential (E_{corr}) (Sastri, 1998).

$$0.5\ O_2 + H_2O + 4e^- \rightarrow 2OH^- \text{ (Reduction reaction)} \quad (2)$$

$$Fe^{++} + 2OH^- \rightarrow Fe\ (OH)_2 \text{ (Ferrous hydroxide)} \quad (3)$$

Ferrous hydroxide is deposited at the anodes (equation 3) and usually converted to various oxide species (the familiar reddish-brown rust) depending on the pH and oxygen availability (equations 4 and 5) (Qian, 2005).

$$4Fe\ (OH)_2 + O_2 \rightarrow 2Fe_2\ O_3.\ H_2O + 2H_2O \text{ (hydrated ferric oxide)} \quad (4)$$

$$6Fe\ (OH)_2 + O_2 \rightarrow 2Fe_3\ O_4.\ H_2O + 4H_2O \text{ (hydrated magnetite)} \quad (5)$$

Corroded rebar expands to 3 to 6 times its original volume, exerting tensile forces within the surrounding concrete. These forces eventually cause delamination (minute fracturing and cracking) just above the rebar mat (Figure 2.2 Krauss, 1996).

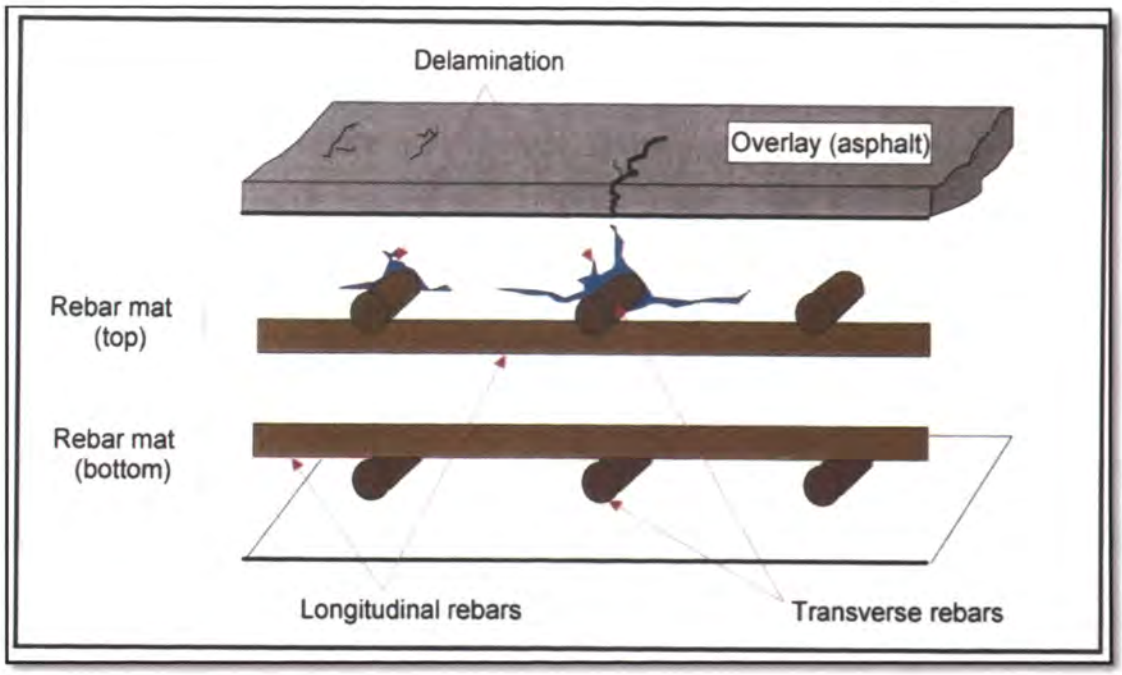

Figure 2.2. Corrosion induced delamination (Krauss, 1996).

2.2.2. Alkali-Aggregate Reaction (AAR). Alkali from the cement paste reacts with silicates in sands and gravels used as concrete aggregate, causing an expansive reaction that leads to cracks in concrete structure. The level of alkali in cement and silicates in aggregates depends on the geological history of their source rock. There are two major categories of AAR, alkali silicate reaction (ASR) and alkali carbonate reaction (ACR) (Jensen, 2005). Of these two reaction types, ASR is the most frequent cause of damage to concrete structures in countries around the world. A fast, expansive ASR reaction is caused by metastable silicates, and it results in severe cracking observable only a few years after construction (Jensen, 2005). A slow, expansive reaction caused by crypto-microcrystaline silicates may not produce visible cracking for up to 20 years. To

prevent AAR, cement can be produced or mixed with pozzolanes (e.g., fly ashes, silica dust) or blast furnace slug (Jensen, 2005). Testing aggregates for reactivity is necessary to ensure that only non-reactive material goes in the mix. Figure 2.3 shows map cracking in a bridge foundation and column caused by ASR.

2.2.3. Cracking. The 1979 TRB report on durability of concrete bridge decks is the primary source for information on bridge deck cracking (TRB, 1979). Cracking is a persistent problem with concrete due to its low tensile strength and the relatively large change in volume that occurs in response to weather changes. Cracking may occur during construction due to shrinking, poor workmanship, or differential settlement as the concrete cures. Although undesired such cracks may not adversely affect the performance of the bridge. The report notes that such cracks can be prevented using shrinkage compensation concrete. Cracking resulting from corrosion, AAR, poor mix ratios, or overloading, however, may occur several years after construction. Cracks of this type may propagate affecting the whole bridge deck as they increase in magnitude and intensity. Eventually the cracking results in complete disintegration of the concrete and loss of bond between the concrete and the reinforcing steel. Further, it speeds corrosion by letting chemicals and water into the internal structure. Thus corrosion exposes more steel, which promotes further cracking. In general, action should be taken to correct crack deterioration when crack thickness exceeds 0.0625 in. (1/16 in.) and when the cracked region covers more than 30 percent of the total deck area (Guthrie and Hema, 2005).

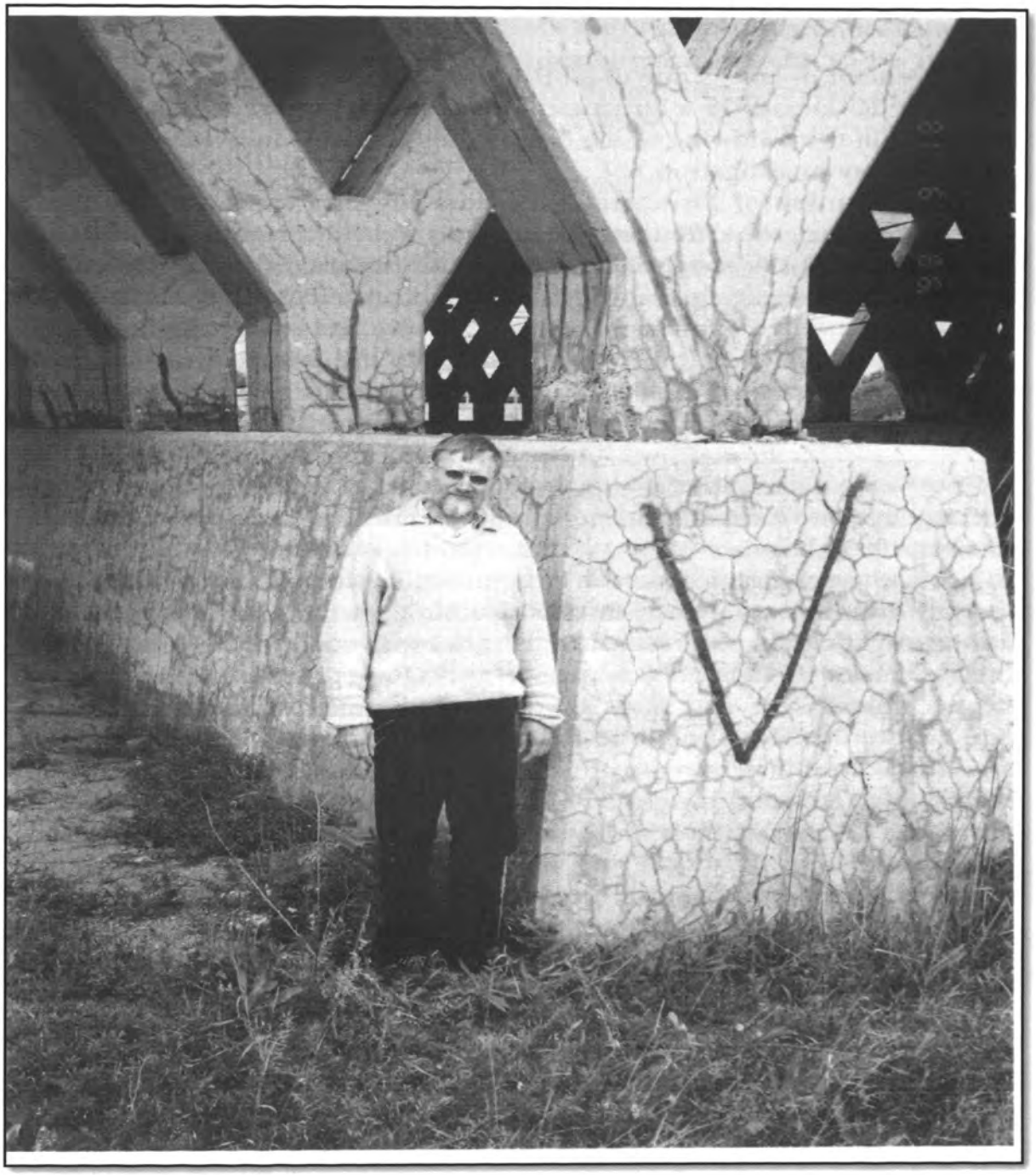

Figure 2.3. Map cracking on a bridge foundation, and Y-column in Canada (Jensen, 2005)

2.2.4. Scaling. The loss of cement paste in concrete exposes the aggregate particles, and at an advance stage both the aggregate and surrounding motor disintegrates into debris. Scaling occurs due to frosting when ice crystals form in the capillaries and pores of the concrete (TRB, 1979). Water in the cement paste is a weak alkali solution, and as the alkali content in the frozen potion creases it creates an osmotic pressure. This pressure causes water to migrate from unfrozen pores to frozen cavities (TRB, 1979). This problem can be addressed with air voids into which the alkali solution flows, reducing the osmotic pressure in the capillaries (TRB, 1979). These voids, however, are counterproductive because they also provide space to hold solution of deicing salt.

2.2.5. Spalling. Corrosion of the reinforcing steel or freezing and thawing circles can cause bursting stresses that exceed the tensile strength of the concrete (Guthrie and Hema, 2005). Spalling mainly follows the direction of the corroded rebar, and in severe cases causes depressions that eventually enlarge into potholes as the concrete is broken down and carried away by moving vehicles, wind, or running water. Spalling can be reduced significantly by increasing the depth of cover over reinforcing steel, lowering the ration of water to cement in concrete, and reducing the amount of de-icing salt (TRB, 1979).

2.3. CONCRETE BRIDGE DECK PROTECTION

Numerous studies have been carried out on different methods of either retarding corrosion or stopping it before it starts, but the success of these methods depends on early diagnosis of the problem. The first sign of corrosion induced deterioration of reinforced concrete is the appearance of reddish brown stains on the surface adjacent to the rebar. The spots enlarge as the rebar expands causing spalling and cracking, and if the structure is not rehabilitated pot holes may occur. Although there are numerous publications on corrosion science and engineering, studies on prevention through inspection and monitoring are very limited (Roberge, 2007). Below is a short description of various ways in which protecting the bridge corrosion can be forestalled or remediated.

2.3.1. Concrete Permeability. Besides strength, durability, and light weight, minimal permeability is among the most desirable properties of a bridge deck. A less permeable bridge deck reduces the amount of chlorides and moisture reaching the reinforcing steel. Permeability can be reduced by proper mix design, by maintenance of a low water/cement ratio during concrete placement, the use of admixtures, by compactive effort, or by application of concrete sealers or coatings (Jesting & Sen, 2003).

2.3.1.1. Concrete Sealers and Surface Coating. Silanes and siloxanes are among the best sealers (Jesting & Sen, 2003). However, rubberized asphalt is also used on already hardened concrete to prevent penetration by chloride. Sealers close the pores of the concrete matrix to prevent liquids from penetrating (Sohanghpurwala, 2006); however, they have poor durability and they do not correct existing problems; therefore, they should not be viewed as a permanent solution. Epoxies, acrylics, methacryate, and

urethane are the primary liquid surface coatings used to prevent water ingress and chlorides diffusion (Sohanghpurwala, 2006).

2.3.1.2. Corrosion-Inhibiting Admixtures. Incorporation of a corrosion-inhibiting admixture (such as calcium nitrate (Jesting & Sen, 2003)) into the concrete is an effective means of controlling corrosion. The amount of chemicals added to the concrete is proportional to the amount of chlorides expected to penetrate to the reinforcing steel, so the effectiveness of the inhibitor is dependent on the accuracy of that prediction (Jesting & Sen, 2003). Although corrosion inhibitors are extensively used, the chemical composition of many is a trade secret guarded by chemical companies (Sastri, 1998). Some inhibitors are known to reduce the rate of corrosion at the cost of compromising the properties of the concrete.

2.3.1.3. Membranes. These are waterproof overlays that protect the concrete of bridge decks from the environment and ingress of chemical elements. Membranes are either in the form of liquid, which can be sprayed on the deck, or preformed sheets, which are bonded to the deck using an adhesive primer (Sohanghpurwala, 2006). Care must be taken when installing membranes to ensure proper bonding between the concrete and the asphalt so that water, moisture, and chemicals cannot accumulate at the interface. A significant disadvantage of membranes is the tendency to cause asphalt to slip on steep grades. In addition, they add dead weight that is not a structural component, and they can develop blisters due to the expansion of entrapped water vapor, leading to potholes (Jesting & Sen, 2003; Sohanghpurwala, 2006).

2.3.2. Epoxy-Coated Reinforcing Steel. Epoxy coating of steel rebar is a fusion encapsulating process whereby hot steel is dipped in epoxy powder and rapidly quenched (Jesting & Sen, 2003). The coating acts as a barrier to corrosion inducing elements; however, it also inhibits proper bonding of the rebar and concrete, and it requires proper handling to avoid damaging the coat (Jesting & Sen, 2003).

2.3.3. Galvanized Reinforcing Steel. Galvanizing does not provide a permanent barrier to corrosion, but it provides a sacrificial coating and consequently has a limited life expectancy when exposed to sufficient quantities of chloride over a long period of time (Jesting & Sen, 2003). When combined with the methods described above, however, galvanizing can significantly increase the life span of a bridge deck.

2.3.4. Cathodic Protection. This is one of the most effective ways of preventing or retarding electrochemical corrosion. The two main methods of cathodic protection are the sacrificial (or galvanic) anode and the impressed current. These methods prevent the corroding anode from discharging ions (Sohanghpurwala, 2006). The sacrificial anode method employs a metal disk that is higher in the electromotive series than the steel rebar to be protected (e.g., zinc or magnesium). This dick is placed in the deck, and corrosion occurs on this metal rather than on the rebar (Jesting & Sen, 2003; Fromm *et al.*, 1979). Impressed current is an external power system that input current to lower the potential of the entire steel rebar. Corrosion is halted when all parts of the rebar are polarized to a potential equal to or greater than the open circuit potential of the most anodic points on the structure (Fromm *et al.*, 1979).

2.3.5. Electrochemical Chloride Extraction. This is a short term concrete treatment similar in principle to cathodic protection; however, the approximate amount of charge applied is 50 to 500 times that used in carthodic protection (Sohanghpurwala, 2006). An electrolyte and an anode are applied on the bridge deck surface and high current is passed between the anode and the reinforcing rebar. The result is an electrochemical reaction where anions migrate from the cathode (or reinforcing steel) toward the anode, while chloride ions migrate away from the steel rebar (Sohanghpurwala, 2006).

2.4. BRIDGE DECK INSPECTION

Since most of the problems with bridge decks occur within the internal structure, which is generally overlaid with asphalt, problems are rarely identified in their early stages. It is important to identify delamination in a timely manner so that less costly remedial process can be implemented effectively. Visual inspection of the entire bridge deck is one of the qualitative methods used to locate deteriorated zones. However, any deterioration at this stage is a manifestation of prolonged internal problems and can be very costly and difficult to repair. Figure 2.4 is an example of deck deterioration visible from the underside of the bridge; Figure 2.4 (a) shows regions of cracking, moisture, and chloride ingress in the slab, and (b) shows deterioration due to water spread caused by unguttered drainage openings.

Repair of deteriorated bridge decks is a complex process constrained by budgetary considerations, weather conditions, and the need to limit traffic disruption; therefore, expedient assessment techniques are needed. Several techniques and various types of equipment (both destructive and non-destructive) are presently available for the assessment of bridge deck condition. Although non-destructive tests are useful for evaluating the state of bridge decks and many other components, they cannot ensure that the tested area will not fail or malfunction (Yahia *et al.,* 2007). Technologies used for detecting deck deterioration includes; sounding (with chain drag, hammer, or steel rod), impact-echo, ultrasonic pulse velocity, infrared thermography, chloride content measurement, corrosion rate measurement, petrographic analysis, and GPR. However, some of these traditional methods are applicable only in the later stages of deterioration

since they cannot detect early internal changes in the concrete. Table 2.3 is a summary of some non-destructive testing methods often used for bridge deck assessment.

(a) Example of severely deteriorated bridge slab.

(b) Deterioration due to unguttered water drainage.

Figure 2.4. Underside view of deterioration on reinforced concrete bridge deck.

Table 2.3. Summary of nondestructive methods for concrete bridge decks (Yehia, *et al*, 2007).

Method	Uses	Advantages	Limitations
Visual inspection	• Cracks • Geometry • Surface roughness	• Accessibility • Oldest known technique • Well established	• Subjective • Time consuming • Qualitative results
Liquid penetrant dye	• Surface flaws • Detection of irregularities	• Portable • Easy interpretation	• Surface preparation • Exhausting for inspector • Time consuming
Chain drag	• Flaw detection inside decks • Delaminations	• Simple • Portable • Good for delaminations	• Time consuming • Tedious • Subjective • Not good with overlays
Half-cell potential	• Detect corrosion state in concrete reinforcement • Corrosion rate	• Simple • Portable • Good for corrosion	• Deck needs preparation • Time consuming • Not good for delaminations • Lane closure • Not very accurate
Acoustic emission	• Cracks • Delaminations • Corrosion	• Real-time response • No lane closures	• Qualitative results only • Not good with overlays • Interpretation • Costly • Not reliable
Ultrasonic pulse velocity	• Homogeneity of concrete cracks, voids • Strength determination	• Portable • Easy test procedure at relatively low cost • Relatively easy to interpret	• Not very reliable for concrete • Attenuation negatively affects results • Does not give information about the shape of defect
Ground penetrating radar	• Concrete mapping, mining, geotechnical, road, and bridge • Forensics • Detection of voids, honeycombing, • Delaminations • Moisture content	• Versatility • Portability • Effectiveness • Low cost • Good with overlays • Minimum traffic control • Prediction of repair quantities in roads	• Interpretation • Complexity of results • Interpretation of results sometimes requires destructive testing
Impact echo	• Detection of voids, cracks, delaminations, unconsolidated concrete, and debonding • Determining thickness	• Requires one surface of the tested material to be exposed, independent of the geometry of the structure • Less susceptible to steel reinforcement • High accuracy	• Size of detected flaws is highly dependent on the impact duration • Less reliable in the presence of asphalt overlays • Interpretation of the results is difficult
Thermography	• Detection of thermal differences, delaminations, cracks, voids	• Portable • Simple, easy interpretation • Minimum traffic interference	• No information about depth of defects • Dependant on environmental conditions

2.4.1. Sounding Methods. Intact concrete produces a sharp ringing sound, and deteriorated zones (i.e. those where there is de-bonding at concrete/asphalt or concrete/rebar level) emit a dull hollow sound when impacted with a hammer, or steel rod, or when a chain is dragged over it (Sohanghpurwala, 2006). This characteristic permits evaluation of concrete by sounding. The traditional chain dragging method is tiresome, time consuming, subjective and is prone to operator error. Furthermore, it is impractical in a noisy environment. However, chain dragging has come of age with the automated chain drag system (ACDS). Using a microphone, this tool records sound produced by dragging chains and uses a computer to analyze the sound, thus distinguishing intact sections of the bridge deck from delaminated sections (Costley, 2005). Figure 2.5 show both automated and manual chain dragging systems employed for both bridge and pavement inspection.

a) The automated chain drag system (ACDS). b) Manual chain dragging.

Figure 2.5 Chain drag systems for bridge and pavement inspection (Costley, 2003).

2.4.2. Impact Echo. This technique uses mechanical impact to produce a stress wave in the material, and reflections occur at interfaces between two materials of differing acoustic impedance (Sohanghpurwala, 2006). The reflected pulse travels back to the receiver transducer and is displayed on an oscilloscope from which the two-way travel time (i.e., the time between impact and receipt of the reflected wave) can be determined. The impact echo technique has proved reliable for locating cracks and other internal defects in concrete; however, it requires good ground-coupling, thus limiting its application on asphalt due to rough the surface and soft asphalt in the summer.

2.4.3. Ultrasonic Pulse Velocity. In principle, this method is very similar to impact echo, differing only in the source of stress wave. Impact echo employs a mechanical source, whereas ultrasonic pulse velocity uses a high frequency transducer to transmit acoustic energy into the concrete. The energy is transmitted or reflected at material interfaces or by internal anomalies and is detected by a receiver transducer. The reflected energy is analyzed in time or frequency domain, and the internal condition of the bridge deck is interpreted based on the pattern and amplitude feature (Roberge, 2007). If the thickness of the material is known, the travel time can be converted into velocity (pulse velocity = path length/transit time) and compared to the known, speed of sound waves in concrete (approximately 12,000 ft per second) (Sohanghpurwala, 2006). This method is affected by temperature changes and moisture content. Further, the rough surface of the asphalt can prevent establishment of proper contact.

2.4.4. Infrared Thermography. Defects within a material will alter the way heat flow is dissipated at its surface (Sohanghpurwala, 2006). Heat flow or transfer from a media of high heat concentration to that of low heat concentration and infrared thermography makes these changes visible. Wind speed, material texture, and surface moisture affect the accuracy of infrared because they affect the way heat is absorbed and dissipated. Infrared is most accurate early in the morning or in the evening just after sunset and its ability to determine the dimensions of any defect is limited.

2.4.5. Chloride Ions Content Analysis. Chloride ions contained in concrete admixtures, de-icing salt and airborne chlorides play an important role in the corrosion of reinforcing steel. Analysis of chloride content is labor intensive and time consuming since it requires core sample drilling at various depths, and milling of samples into powder for analysis. Field test kits have been developed; however, they are less accurate than laboratory results and can only serve to corroborate the lab results. In general, state DOTs require action when chloride concentrations exceed a threshold of 2.0 lbs/yd^3 of concrete (Guthrie and Hema, 2005). Chapter 4 addresses chloride ion analysis in greater details.

2.4.6. Corrosion Rate Measurement. The higher the rate of corrosion, the sooner cracking and spalling will occur. Knowing the rate at which corrosion occurs, therefore, is vitally importance in estimating repair time and determining the preventive measures to be applied. This method involves application of a small voltage to the reinforcement; the output voltage or current is then measured. High currents indicate a high rate of corrosion of the reinforcing rebar. Although corrosion rate measurement has

been used in the electrochemical laboratories for decades, it has only recently been applied in the field (Sohanghpurwala, 2006).

2.4.7. Petrographic Analysis. Core sample from a bridge maybe examined microscopically for deterioration. Information obtained by such analysis includes material condition, degree of cement hydration deterioration caused by chloride corrosion, and probable future performance (Sohanghpurwala, 2006). Like chloride ions content analysis, this method is time consuming and must be performed by a specialist.

2.4.8. Ground Penetrating Radar. This technique is gradually becoming the work horse of bridge deck survey. Its increased application and success in bridge inspection is due to numerous improvements in data acquisition and processing software. The present study relies primarily on GPR.

3. GPR BACKGROUND

3.1. HISTORY

Daniels books on radar are the primary source for the information on the history of GPR (Daniels, 1996 and 2004). Ground penetrating radar (i.e., radio detecting and ranging) is also referred to as ground probing radar or georadar. It operates by transmitting a short pulse of electromagnetic energy into the surface and recording reflection from material interfaces. Since its inception, GPR has improved tremendously in terms of data acquisition, data processing techniques, and application.

The first use of electromagnetic (EM) signals to determine the presence of remote terrestrial metal objects is generally attributed to Hulsmeyer in 1904, but the first description of their use for locating objects in the subsurface did not appear until six years later in a German patent by Leimbach and Lowy (Daniels, 2004). They used a transmitter and a receiver antenna similar to those used today; however, Leimbach and Lowey developed a crude image of the subsurface by burying dipole antennas in an array of vertical boreholes and comparing the magnitude of received signal when each successive pair were used to transmit and receive.

In 1926, noting that the dielectric variations in subsurface material affected signal reflection, Hulsenbeck used the modern pulse technique to investigate the nature of buried features. The full development of pulse technique took off from the 1930's onwards as a means to investigate depth in ice, fresh water, salt deposits, desert sand and rock formations, and rock and coal deposits (Daniels, 1996); however, enormous signal attenuation in some material made its application in some fields impractical. Interest in

GPR increased again in the mid-1970s with the lunar investigation and landing expeditions (Daniels, 2004).

Pavement thickness can sometimes be determined by consulting road construction records; however, such records are often unavailable or incomplete. When pavement thickness must be measured, it is typically determined by drilling, but coring is time consuming and destructive. Since the early 1980s GPR has been successfully used to evaluate pavement. North America, and Scandinavia were the main regions where GPR technology was improved. The Unites States FHWA is credited for development of the first vehicle mounted GPR system for use on roads in 1985; in Scandinavia by the late 1980's ground-coupled GPR had become a routine tool in road maintenance projects (Evans *et al.*, 2008).

Application of electromagnetic (EM) signals have expanded significantly, their use in GPR include building and structural nondestructive testing (NDT), archaeology, glaciology, hydrology, roadway and tunnel quality investigations, buried utilities location, land mines and unexploded ordinance detection, and remote sensing by satellite. Table 3.1 provides a comprehensive list of GPR applications in various scientific fields. Incremental but consistent improvements in GPR technology have increased its accuracy and encouraged the developer of hardware and data processing software, making GPR a very versatile tool.

Table 3.1. Range of GPR application (Reynolds, 1997).

Geological:
Detection of natural cavities and fissures
Subsidence mapping
Mapping sand body geometry
Mapping of superficial deposits
Soil stratigraphy mapping
Glacial geological investigations
Mineral exploration and resource evaluation
Peat thickness mapping and resource evaluation
Permafrost investigations
Location of ice wedges
Fracture mapping in rock salt
Location of faults, dykes, coal seams, etc.
Geological structure mapping
Lake and riverbed sediment mapping

Environmental:
Contaminant plume mapping
Mapping and monitoring pollutants within groundwater
Landfill investigations
Location of buried fuel tanks and oil drums
Location of gas leaks
Groundwater investigations

Glaciological:
Ice thickness mapping
Determination of internal glacier structures
Ice movement studies
Detection of concealed surface and basal glacier crevasses
Mapping water conduits within glaciers
Determination of thickness and type of sea and lake ice
Sub-glacial mass balance determination
Snow stratigraphy mapping

Engineering and construction:
Road pavement analysis
Void detection
Location of reinforcement (rebars) in concrete
Location of public utilities (pipes, cables, etc.)
Testing integrity of building materials
Concrete testing

Archaeology:
Location of buried structures
Detection and mapping of Roman Roads, etc.
Location of post-holes, etc.
Pre-excavation mapping
Detection of voids (crypts, etc.)
Location of graves

Forensic science:
Location of buried targets (e.g. bodies and bullion)

3.2. ELECTROMAGNETIC (EM) THEORY

3.2.1. EM Classification. Any current carrying conductor has a weak magnetic field around it; however, the magnetic field strength can be significantly increased if the current carrying conductor is made into a loop with many turns.

As shown in Figure 3.1, the frequency of EM radiation ranges from atmospheric micropulsation (less than 10Hz) to radar band (108 to 1011 Hz), to X-rays and gamma-rays (in excess of 1016Hz) (Reynolds, 1997). The frequency of the GPR pulse energy ranges from 10 MHz to several thousand MHz, this frequency it is known as microwave radiation, or more commonly, radar. (Reynolds, 1997)

3.2.2. EM Waves. Although EM waves are three dimensional, for most GPR applications they are considered as propagating in two dimensions (2-D) since the analysis of the third dimension is redundant when using reciprocal antennas (Baker *et al.*, 2007). The two components, electric (*E*) and magnetic (*H*), are perpendicular to the direction of travel (x) (Figure 3.2). EM energy is self-propagating energy composed of conjoined oscillating electrical and magnetic fields require no transport medium. In general, EM waves propagate through air and free space at a constant speed comparable to the speed of light, but their magnitude attenuates when they encounter a medium that reflects or absorbs them. In free space (i.e., a vacuum), both the electrical and magnetic components of EM waves are in phase and travel at speed of light (Conyers, 1997). In real material, they are out of phase; their propagation velocity drops and they are not completely polarized (Kim, 2003).

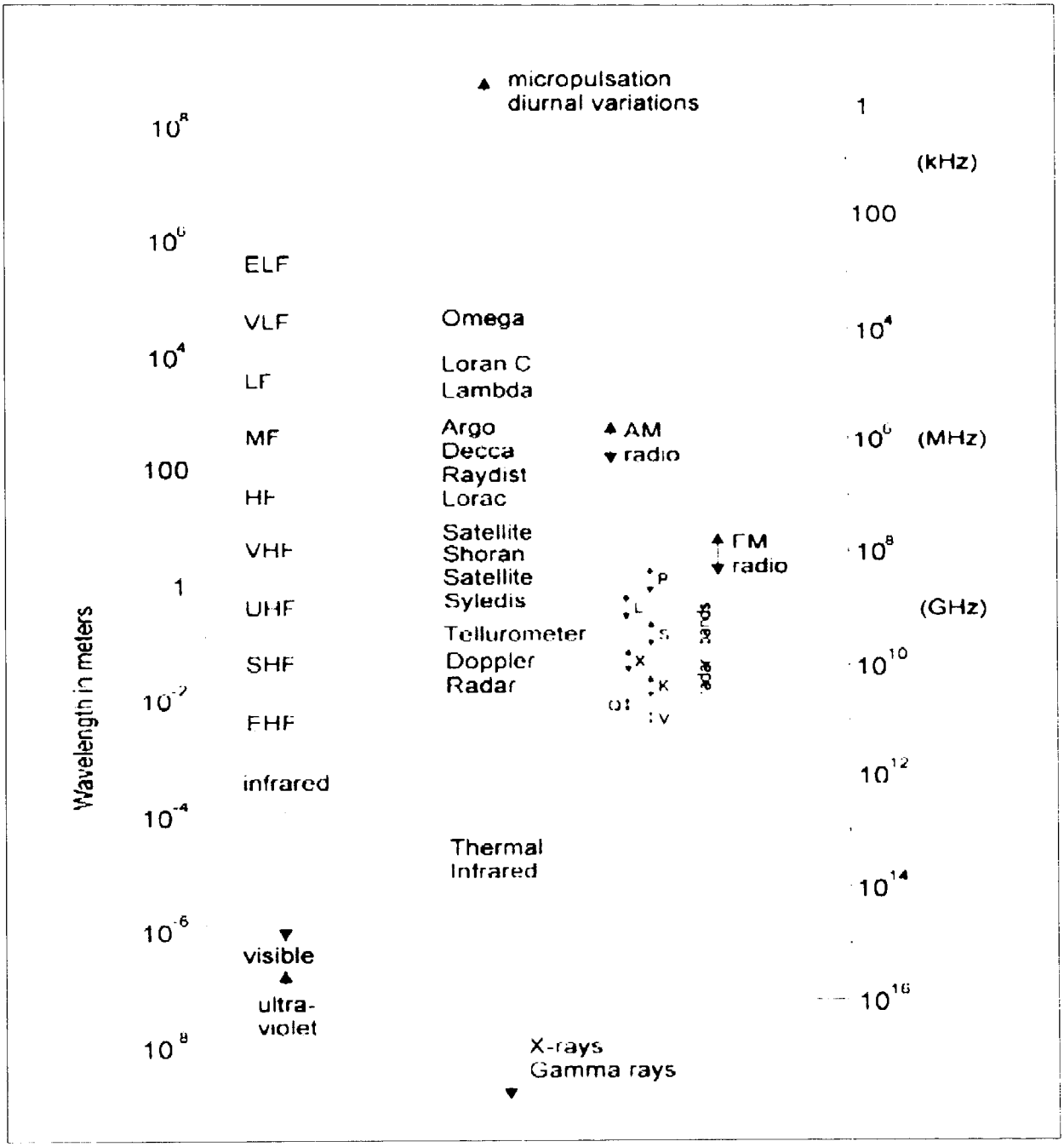

Figure 3.1. Electromagnetic spectrum (Reynolds, 1997).

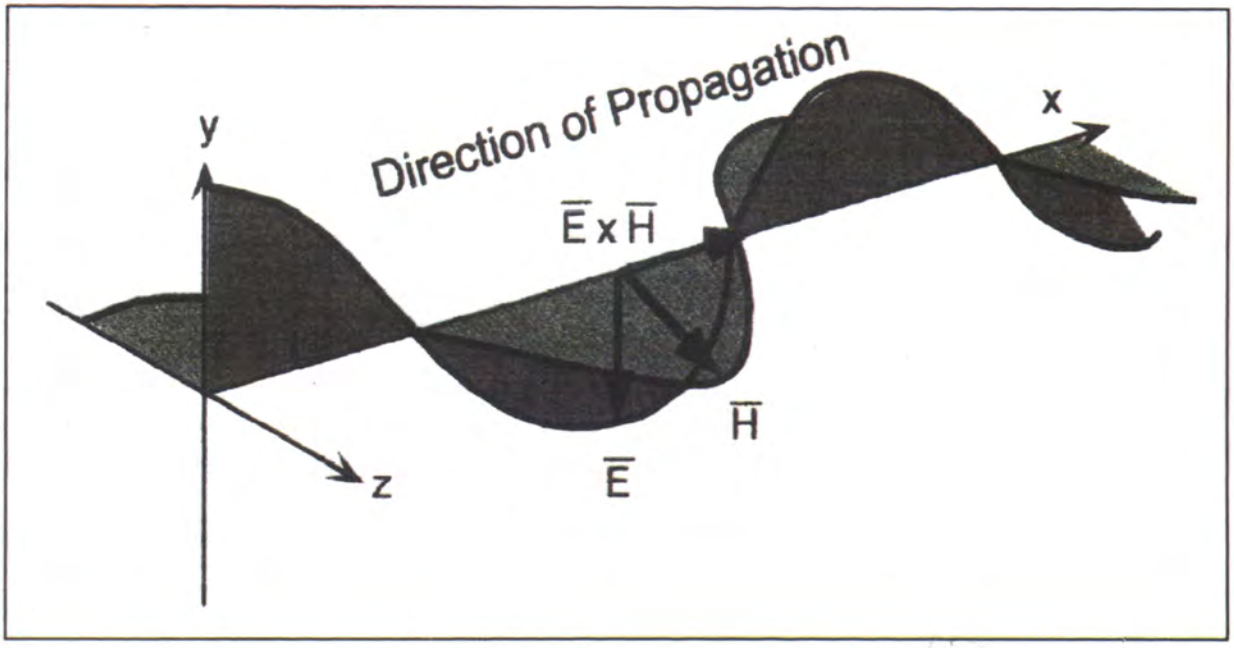

Figure 3.2. Basic elements of an electromagnetic wave, showing the two principle electric (*E*) and magnetic (*H*) components (Reynolds, 1997).

3.3. GROUND PENETRATING RADAR (GPR) THEORY

3.3.1. Principles of Operation. A ground penetrating radar (GPR) unit consists of a transmitter and a receiver antenna. GPR operates by transmitting short pulses EM energy ($\leq$ 1 ns ($1*10^{-9}$ s) from a transmitter antenna into the subsurface and recoding reflections from material interfaces or internal anomalies to a receiver antenna (Figure 3.3a) (Maierhofer, 2003). Data collected by GPR has four main components: a) changes in reflection strength, b) changes in arrival times of specific reflections, c) source wavelet distortion, and d) signal attenuation (Cardimona *et al*, 2001). The total required for short pulse EM energy to travel into the subsurface and be reflected back to the receiver antenna is called the arrival time (sometimes called two-way travel time or round-trip travel time). The arrival time is used to determine the propagation velocity of the subsurface material using the relation (Velocity = distance / travel time).

When GPR is used to assess rebar reinforced in concrete, the profiles are oriented perpendicularly to the rebar. The GPR beam and the rebar result in hyperbolic shaped image (Figure 3.3b) which visually looks like an inverted U. The hyperbolic reflection appears somewhat distorted if the GPR profile is not perpendicular to the linear target (Kim, 2003). If the orientation of the survey lines is parallel or nearly parallel to a linear target, the reflection appears as a slightly curved line or a continuous layer, in this case test runs necessary to ascertain the orientation of the linear targets (Kim, 2003). The hyperbolic shape is generated because the transmitter antenna radiates an elliptical cone shaped beam (Figure 3.4) that spreads as it gets further from the source. Consequently, the received reflection from the rebar has a decreasing arrival time (or decreasing depth) as the antenna approaches the apex of the rebar. The arrival time then increasing after the

antenna passes over the rebar (Figure 3.5) (GSSI MN-72-433, 2007). The peak of the hyperbola indicates the apex of the object in the ground (i.e., of the rebar in concrete). This peak represents shortest arrival time. The hyperbola can be migrated (moving each beam to the apex) so that the target appears as a point, increasing the accuracy of the relative amplitude value.

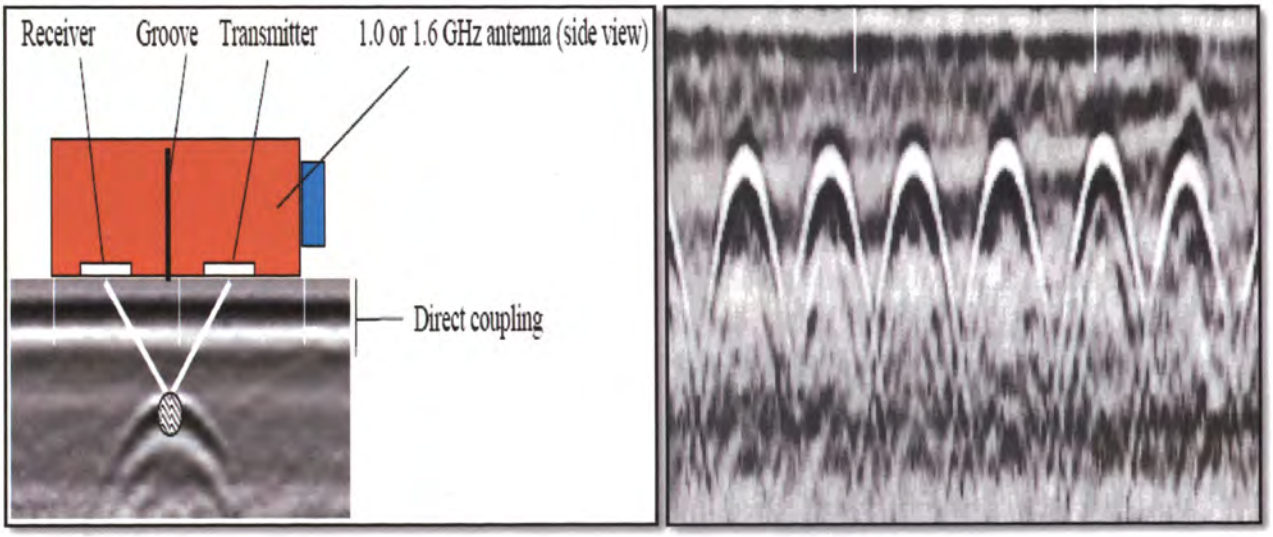

a) Target location. b) *Hyperbolic* shaped images of rebar mat.

Figure 3.3. a) Location of a target (GSSI Handbook, 2005) and b) *hyperbolic* (inverted U) shaped images associated with linear targets.

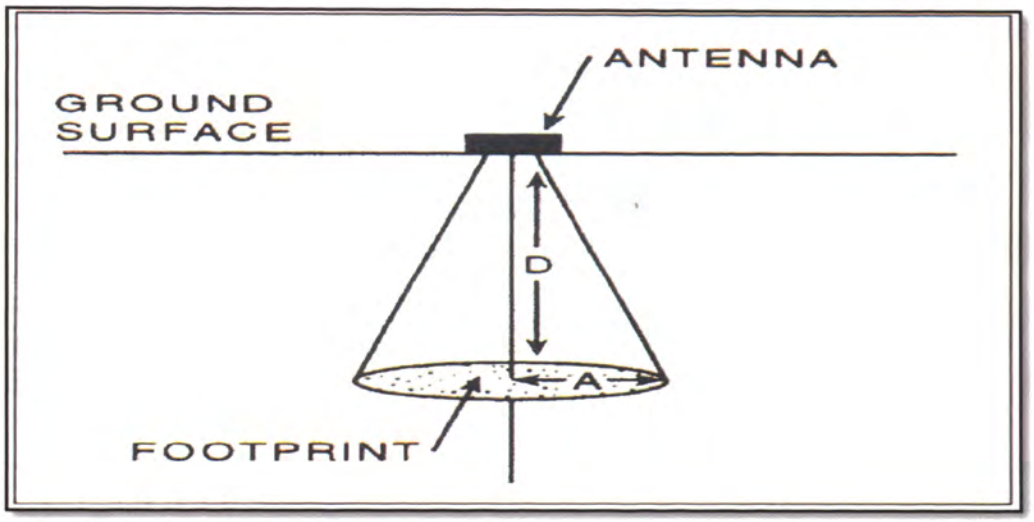

Figure 3.4. Elliptical cone of GPR penetration (Conyers, 1997).

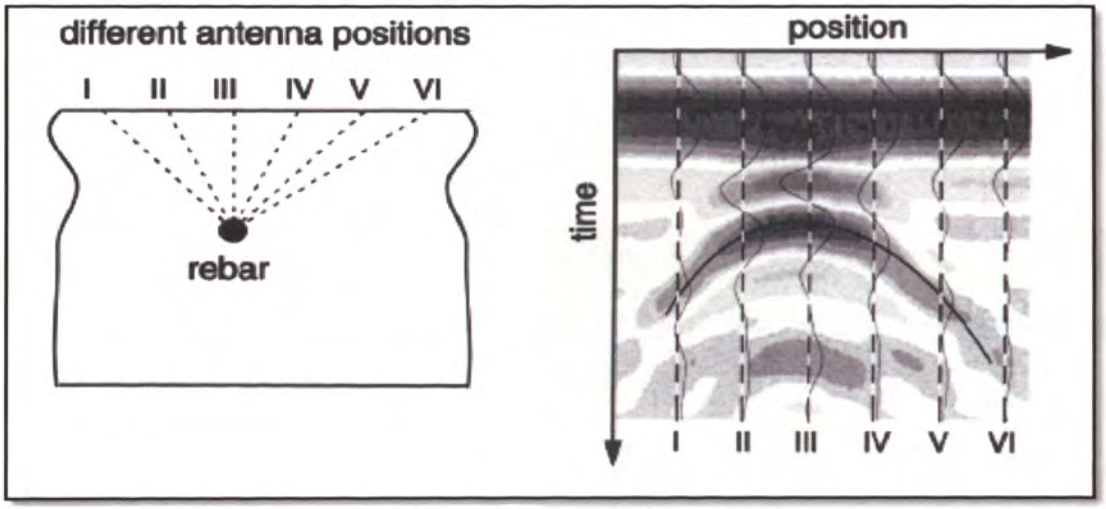

Figure 3.5. Development of a GPR hyperbolic signature (Maierhofer, 2003).

3.3.2. Physical Parameters. EM properties that affect the propagation of radio waves include dielectric constant (ε), magnetic permeability (μ) and electrical conductivity (δ). Magnetic permeability (μ) becomes significant only in a ferromagnetic medium (Baker *et al.*, 2007). Variations in EM properties of material are caused by physical factors such as, lithology, porosity, water content, and water salinity.

Dielectric constant (ε) is the ability a medium to store EM energy in the form of induced charge polarization and then permit to the passage of EM energy when an external field is imposed on the material (Conyers,1997). Dielectric constant also referred as dielectric permittivity is commonly represented by the relative dielectric constant (ε_r), which is the ratio of the dielectric constant of a material to the dielectric constant of free space (Equation 1) (Kim, 2003).

$$\varepsilon_r = \frac{\varepsilon}{\varepsilon_0} \quad \text{[dimensionless]}, \tag{1}$$

where $\varepsilon_0 = 8.854 * 10^{-12}\ F/m$

Change in the dielectric contestant of a material depends primarily on the water content of that material (Daniels, 1996).

Magnetic permeability (μ) measured in henry/m, is the ability of material to store (or get magnetized) and dissipate when EM field is imposed on it (Baker *et al.*, 2007; Sheriff, 1984). Magnetic permeability is a complex number with the real part describing the storage component and the imaginary part describing the dissipation component (Equation 2) (Baker *et al.*, 2007).

$$\mu_r = \frac{\mu}{\mu_0} \text{ [dimensionless]} \quad (2)$$

Slightly magnetic or non-magnetic materials (i.e., most rocks and soils) have very little effect on the propagation of EM waves, the value of $\mu \approx \mu_0$, hence their relative permeability is approximately equal to one (Baker *et al.,* 2007; Kim, 2003). However, media that contain magnetic minerals, iron-oxide cement, and iron-rich soils have a relative magnetic permeability high enough to attenuate EM energy during transmission (Kim, 2003).

Electrical Conductivity (δ) is the ability of a medium to transport electric charges (Sheriff, 1984) (or simply a measure of the ease at which electric movement within a material is achieved). In highly conductive medium (e.g., saltwater and, high clay content soils) the electrical component of EM energy is essentially conducted into the earth and becomes lost because the total EM field is composed of electrical and magnetic fields, dissipating one of them leads to attenuation (Kim, 2003). Table 3.2 shows electrical properties of some natural and manmade materials and their effect on attenuation of EM waves. A medium of high dielectric constant, low electric conductivity, and low magnetic permeability has little effect on EM energy attenuation.

Table 3.2. Attenuation and electrical properties of various materials measured at 100MHz frequency (Daniels, 2004).

Material	Attenuation (dB/m)	Conductivity (S/m)	Dielectric Constant
Air	0	0	1
Asphalt: dry	2-15	10^{-3}-10^{-2}	2-4
Asphalt: wet	2-20	10^{-2}-10^{-1}	6-12
Clay: dry	10-100	10^{-3}-10^{-1}	2-6
Clay: saturated	10-100	10^{-1}-1	15-40
Concrete: dry	2-12	10^{-3}-10^{-2}	4-10
Concrete: wet	10-25	10^{-2}-10^{-1}	10-20
Freshwater	0. 1	10^{-4}-10^{-2}	81
Freshwater ice	0. 1-2	10^{-3}	4
Granite: dry	0. 5-10	10^{-8}-10^{-6}	5
Granite: wet	2-5	10^{-3}-10^{-2}	7
Limestone: dry	0. 5-10	10^{-9}-10^{-6}	7
Limestone: wet	10-25	10^{-2}-10^{-1}	8
Sand: dry	0. 01-1	10^{-7}-10^{-5}	4-6
Sand: wet	10-100	10^{-4}-10^{-2}	10-30
Sandstone: dry	2-10	10^{-9}-10^{-6}	2-3
Sandstone: wet	10-20	10^{-5}-10^{-6}	5-10
Seawater	1000	4	81
Seawater ice	10-30	10^{-2}-10^{-1}	4-8
Shale: saturated	10-100	10^{-2}-10^{-1}	6-9
Soil: sandy dry	0. 1-2	10^{-4}-10^{-2}	4-6
Soil: sandy wet	1-5	10^{-2}-10^{-1}	15-30
Soil: loamy dry	0. 5-3	10^{-4}-10^{-3}	4-6
Soil: loamy wet	1-6	10^{-2}-10^{-1}	10-20
Soil: clayey dry	0. 3-3	10^{-2}-10^{-1}	4-6
Soil: clayey wet	5-30	10^{-1}-1	10-15

3.3.3. EM Wave Propagation Velocity and Frequency. Dielectric constant is an important parameter that controls the EM propagation velocity (Baker *et al.*, 2007) and hence has an influence on frequency (equations 3 and 4). The velocity at which EM energy propagates through a media can be derived or measured. For homogeneous and isotropic material, the relative propagation velocity can be calculated from equation (3) (Daniels, 2004).

$$v = \frac{c}{\sqrt{\varepsilon_r}} \text{ [m/s]}, \tag{3}$$

$$\gamma = \frac{v}{f} \text{ [m]}, \tag{4}$$

Where v = speed of radio wave in a material (m/ns),

C = speed of light in free space (3 * 108 m/ns),

ε_r = relative dielectric constant,

γ = wavelength (m), and

f = frequency in (hertz) (Baker *et al.*, 2007).

Equation (3), demonstrates that materials with low dielectric constant have a high propagation velocity, and equation (4) shows that wavelength decrease as the velocity decreases. These equations, however, are true only for a perfect dielectric medium, and apply to real dielectric media only with some assumptions. A perfect dielectric medium is one in which both magnetic susceptibility and electric permittivity are constant (Daniels, 1996).

When dielectric constant is not known, the velocity of EM propagation can also be calculated by means of multiple measurements from a hyperbolic spread function (as shown in Figure 3.5) using equation (5).

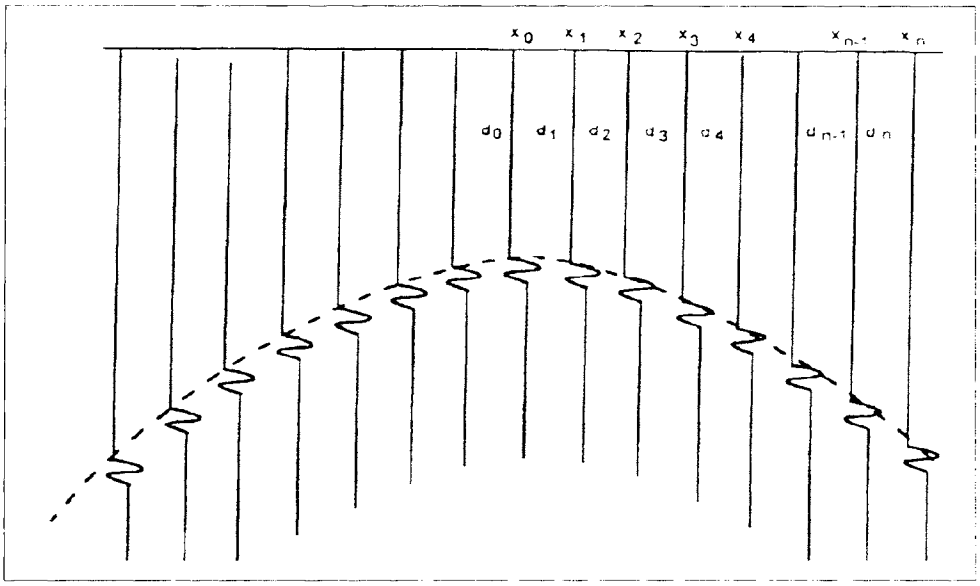

Figure 3.6 Hyperbolic spread function (Daniels, 1996).

$$v_r = 2\sqrt{\frac{x_{n-1}^2 - x_n^2}{t_{n-1}^2 - t_n^2}} \quad (5)$$

Where x_n = scan spacing,

t_n = the arrival time from the surface to the diffraction at the n^{th} distance from the center of diffraction.

3.3.4. Depth Estimation. After establishing the velocity at which radar energy propagates through the ground, and after measuring the arrival time of the pulse is, the depth to the target can be accurately derived. However, this calculated depth should be calibrated using either a target buried at a predetermined depth or from the hyperbolic spread function (Figure 3.6) (Kim, 2003).

3.3.4.1 Depth calculation. High frequency antennas are employed where resolution is of great importance; however, this is a trade off with depth and vice versa. GPR penetration depth is a function of moisture content, salt content, number of reflection and scattering centers, the frequency of the EM wave, and the opening angle of the antenna (Maierhofer, 2003). Assuming a perfect dielectric medium, the arrival time can be converted into depth or thickness using equation (6).

$$d = \frac{vt}{2} \tag{6}$$

where, d = depth to the target (m),

v = velocity of EM wave in a media (m/ns), and

t = two-way travel time (ns).

Alternatively distance can also be calculated using the velocity and time from the hyperbolic spread function (equation 7):

$$d_0 = \frac{v_r\, t_0}{2} \tag{7}$$

3.3.5. Reflection and Transmission Coefficients. The incident EM energy undergoes several changes as it travels through the medium, but of particular importance for the present discussion is the reflected and transmitted energy. Dielectric contrast between two adjacent layers causes reflection or diffraction of the some EM energy while the remainder is transmitted to the bottom layer. Table 3.3 shows that the strength (or brightness) of a reflection is proportional to the dielectric constant between two materials. This table further indicates that the greater the contrast between two adjacent media, the stronger the reflection.

Table 3.3. Dielectric contrasts between different media and resulting reflection strength (GSSI MN72-367 Rev. D, 2005).

Boundary	Dielectric contrast	Reflection strength
Asphalt-concrete	Medium	Medium
Concrete-sand	Low	Weak
Concrete-air	High. phase reversal	Strong
Concrete deck-concrete beam	None	No reflection
Concrete-metal	High	Strong
Concrete - water	High	Strong
Concrete - PVC	Low to Medium. phase reversal	Weak

If the dielectric constant of the two media is known, equation (3) can be used to calculate the velocities of the two layers. The magnitude of reflected energy can be calculated using equation (8):

$$R = (v_1 - v_2) / (v_1 + v_2) \tag{8}$$

where v_1 and v_2 are EM velocities in layers 1 and 2 respectively where $v_1 < v_2$ (Kim, 2003).

Calculation of the reflection coefficient is complicated when the dielectric constant increases or decreases across the interfaces and when the layers are thin (i.e., less than one-quarter of the wave length) (Baker *et al.*, 2007). From Equation (3)

velocity is inversely proportional to the dielectric constant of the medium; therefore reflection coefficient (R) can also be calculated using the dielectric constant (equation (9):

$$R = \frac{\sqrt{\varepsilon_1}-\sqrt{\varepsilon_2}}{\sqrt{\varepsilon_1}+\sqrt{\varepsilon_2}} \quad (9)$$

Where ε_1 and ε_2 are dielectric constants of layer 1 and 2 respectively, applicable for incidence at right-angle to a plane reflector; typically, $\mathcal{E}_r$ increases with depth (Reynolds, 1997).

EM energy transmitted at the interface of two adjacent layers is dependent upon the magnetic permeability and the dielectric constant of the respective layers. The amount of energy transmitted to the lower layer can be described by the transmission coefficient (t) (Lorrain and Carson, 1970) (equation 10).

$$t = \frac{2(\frac{\mu_2}{\varepsilon_2})}{(\frac{\mu_2}{\varepsilon_2})+(\frac{\mu_1}{\varepsilon_1})} \quad (10)$$

where $(\frac{\mu_2}{\varepsilon_2})$ and $(\frac{\mu_1}{\varepsilon_1})$ are intrinsic impedance of the bottom and top layer respectively.

3.4. ANTENNA CHOICE

Although antenna capability is limited by the properties of the material, data quality, penetration depth, and resolution are controlled by the antenna frequency. In general, the choice of antenna can be roughly classified by application into two categories which include geological and engineering non-destructive (NDT) survey. Frequencies less than or equal to 500MHz are used for geological applications in which depth of penetration is more important than fine resolution. Frequencies above 500MHz, and preferably above 900MHz, on the other hand are employed in engineering NDT testing (Reynolds, 1997). Table 2.4 shows antenna choices for geological and engineering NDT applications.

Table 3.4. Various antenna frequency applications (GSSI SIR-3000 Users Manual, 2006).

Frequency	Sample Applications	Typical Max Depth Feet (meters)	Typical Range (ns)
1.6 GHz	Structural Concrete, Roadways, Bridge Decks	1.5 (0.5)	10-15
900 MHz	Concrete, Shallow Soils, Archaeology	3 (1)	10-20
400 MHz	Shallow Geology, Utility, Environmental, Archaeology	9 (3)	20-100
200 MHz	Geology, Environmental	25 (8)	70-300
100 MHz	Geology, Environmental	60 (20)	300-500

3.5. ENERGY LOSS OR ATTENUATION

Attenuation is the loss or dissipation of energy as radiowaves travel from the source through the subsurface. This is analogous to the loss of cell phone signal when driving through a tunnel and it is dependent on the nature and thickness of the overburden on the tunnel. The signal detected by the receiver undergoes numerous losses (Figure 3.7) during its transmission. This energy loss occurs due to factors such as, geometric spreading, ground coupling effects (transmission-coupling and retransmission-coupling loss), scattering, material loss, antenna loss, and transmission loss (due to moving charged particles).

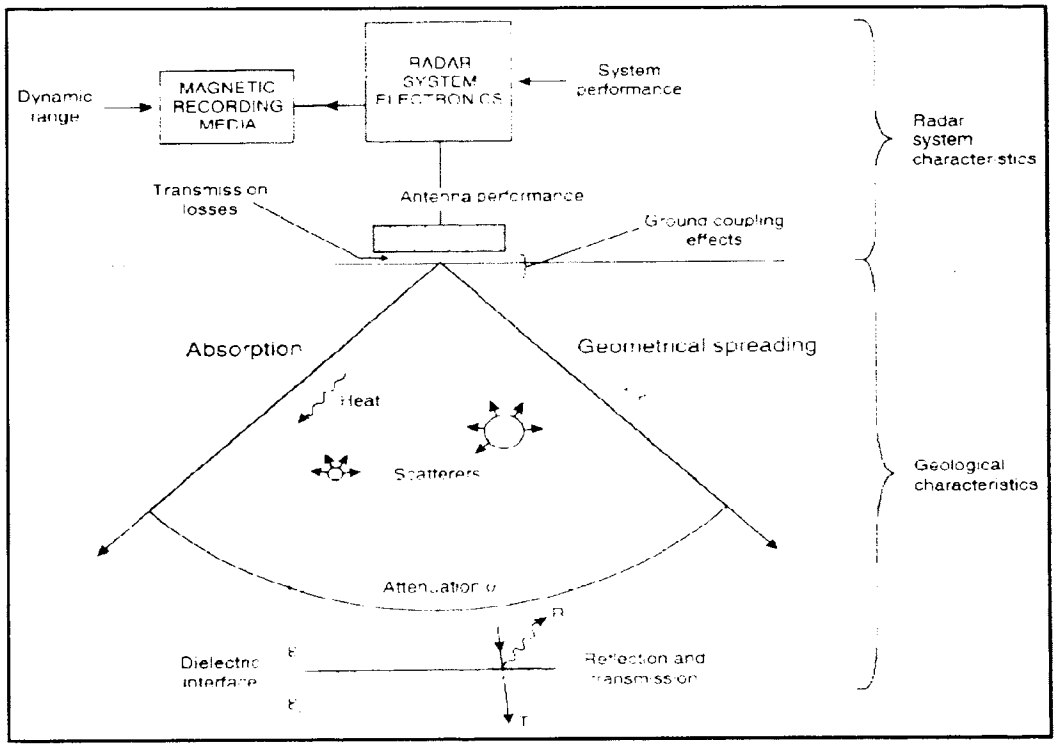

Figure 3.7. Processes that lead to signal attenuation (Reynolds, 1997).

3.5.1. Geometric Spreading or Spherical Divergence. Spherical spreading occurs as the EM energy propagates away from the transmitter, resulting in the weakening of the radar signal. Although the radius increases further from the source the energy output does not increase; therefore, the energy per unit area reduced with time.

3.5.2. Ground Coupling Effect. This is the energy loss that occurs when there is an air interface between the transmitter/receiver antenna and the surface. The amplitude of the signal changes as it travels through the air media (transmission-coupling loss). This air interface also affects the signal on its return journey to the receiver (retransmission-coupling loss).

3.5.3. Antenna Loss. Attenuation of the antenna input starts within the equipment itself. Like electrical appliances and machines, antennas are not 100% efficient. Antenna loss, therefore, can be simply termed as the comparison between the applied energy (input) and the energy available for radiation (output). Resistivity of antenna electrical component reduces efficiency by converting some energy into heat, and some energy is used to move charge.

3.5.4. Scattering. This is the irregular and diffuse dispersion of the energy caused by inhomogenities in the medium through which the energy propagates (Sheriff, 1984). Although scattering contributes to energy loss, without it the GPR receiver antenna would not have any measurements to record. Each time a wave passes through an interface, or if there are objects with dimensions of the same order as the wavelength of the radar signal, energy will scatter in a random manner. This scattering causes noise in the radar data and is called Mei scattering (Reynolds, 1997).

3.5.5. Material Loss. Attenuation loss of a material is a complex function (difficult to obtain) of both dielectric and electrical properties of the medium through which EM energy propagates (Webb, 2000). However, an approximation of intrinsic attenuation value of a given material can be calculated by,

$$\alpha = -16\ 37(\sigma/\varepsilon), \tag{11}$$

Where α = approximate attenuation value,

σ = conductivity of the medium and,

ε = material dielectric constant (Lucius and Powers, 1997).

Natural occurring clays are as significant attenuators and it is mostly concluded that GPR is not applicable in this environments. It should be noted that nonclay but clay-sized material (i.e., fresh glacial rock flour) do not attenuate signal to the degree observed in naturally occurring clays; thus, it is not true to say that all clay sized material strongly attenuate GPR signal (it is the fraction of naturally occurring clay that is important) (Baker *et al.*, 2007). Table 3.5 presents material loss for selected medium.

Table 3.5. Typical range of loss for various materials at 100 MHz and 1 GHz (Daniels, 1996).

Material	Loss at 100 MHz	Loss at 1 GHz
Clay (moist)	5–300 dB/m	50–3000 dB/m
Loamy soil (moist)	1–60 dB/m	10–600 dB/m
Sand (dry)	0.01–2 dB/m	0.1–20 dB/m
Ice	0.1–5 dB/m	1–50 dB/m
Fresh water	0.1 dB/m	1 dB/m
Sea water	1000 dB/m	10 000 dB/m
Concrete (dry)	0.5–2.5 dB/m	5–25 dB/m
Brick	0.3–2.0 dB/m	3–20 dB/m

4. GPR FOR BRIDGE DECK ASSESSMENT

Transportation agencies are constantly searching for more efficient, expedient, and cost-effective methods for assessing subsurface conditions of their transportation facilities. Of all the technologies currently available, GPR is the most promising nondestructive tool with a variety of applications. The use of GPR for evaluating subsurface conditions of transportation infrastructure has been on the rise in United States, Canada, and parts of Europe.

When applied for bridge deck assessment different signatures in the GPR profile may be used for detecting corrosion of steel reinforcement within the concrete deck, which can indicate poor quality overlay bonding or delamination at the rebar level. Intact rebar has very high reflection amplitude and visually clear hyperbolic shape; however, corroded rebar leads to significant attenuation of the reflected GPR signal. Figure 4.1 shows various bridge conditions, including a) zones of intact rebar, b) severely deteriorated areas where rebar appear missing due to total signal attenuation, and c) mildly deteriorated regions where the rebar reflection is low. Another effect of corrosion and delamination on GPR signal is the late arrival times of reflections (i.e., increased travel time) due to reduction of signal velocity, which makes the affected rebar appear to be deeper than the intact rebar. Low signal strength (or reflection amplitude). Longer arrival time (i.e., increased vertical distance to the rebar) result from increased dialectic constant (i.e., decreased electromagnetic velocity) which is also indicative of deterioration.

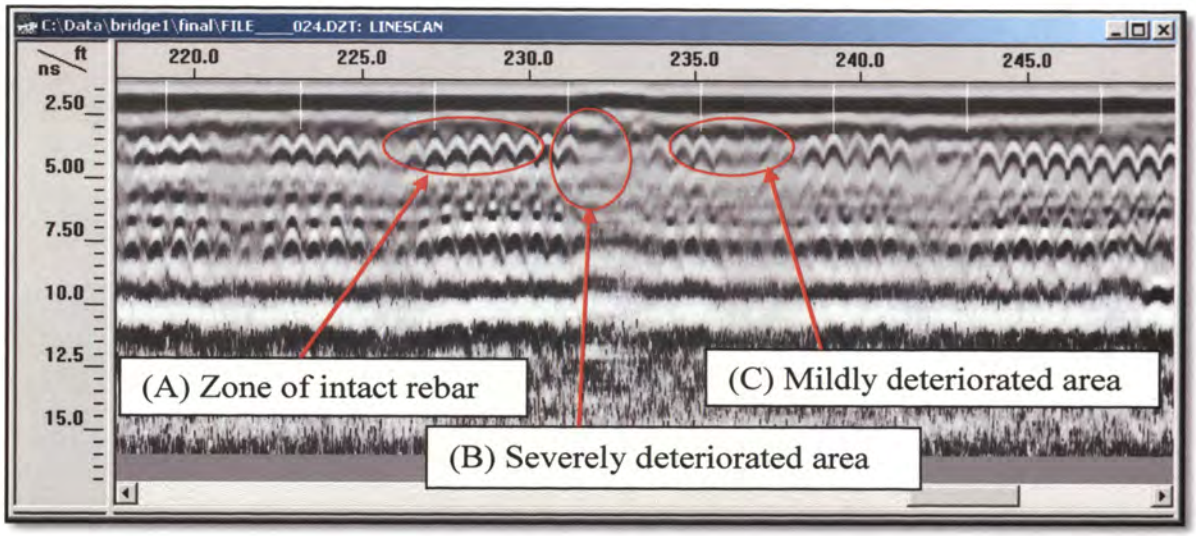

Figure 4.1. Characteristics of a deteriorated bridge deck.

The use of rebar reflections as a measure of attenuation requires that the density of transverse rebar be uniform. Also, if there is significant moisture at the asphalt/concrete interface due to poor bonding, the amount of energy reflected is high due to the high dielectric constant associated with the moisture and chloride. This condition will produce variable reflections at the asphalt/concrete boundary (Kim, 2003). Both moisture and chlorides are necessary for corrosion, their presence correlates with rebar corrosion and ultimately with delamination. This correlation, however, can be misleading because moisture and chloride in the deck may not have migrated to the depth of rebar mat. The success of GPR on bridge deck assessment is dependent on the antenna frequency. Antennas are designed for either air-coupled or ground-coupled operation (Figure 4.2).

(a) 2 GHz air-launched antenna. (b) 1.6 GHz ground-coupled antenna.

Figure 4.2. Antennas for pavement inspection (GSSI, website).

Air-launched antennas provide for rapid data collection, although at the expense of resolution. Ground-coupled antennas provide excellent resolution but slow data acquisition speed. According to Reynolds simple classification of antenna by application (1997) high frequency antennas are applied where resolution is preferred to depth. Application of 1.5 GHz ground-coupled antenna, by Missouri University of Science and Technology formerly University of Missouri- Rolla and Missouri department of transportation (MDOT) in1999 and 2005 study by Main DOT and Geophysical Survey Systems indicate that high frequency antennas return high resolution of the upper rebar mat and layers within a bridge deck.

4.1. PROJECT SCOPE AND BRIDGE DECK DESCRIPTION

This project employed a GSSI SIR System-3000 and a 1.5GHz model 5100 antenna on two asphalt-covered concrete bridges, Bridge A-090-0095, and Bridge C-(048-0011 and 048-0012) and one concrete bridge, Bridge B-090-0087. The 1.5GHz antenna was selected because of the need of high resolution for small targets such as rebar. The orientation of the GPR profiles was perpendicular to the orientation of reinforcing rebar (i.e., in the direction of traffic travel). The profile spacing varied depending on the amount of visible deterioration. In areas perceived to be more deteriorated the spacing was closer than in the areas where deterioration appeared minimal. The GPR signature indicates that these three concrete bridges are reinforced with two rebar mats (top and bottom) and that each rebar mat has both longitudinal and transverse rebars.

4.2. DATA ACQUISITION PARAMETERS

A successful GPR bridge deck survey requires a general understanding of radar principles, proper use of equipment, proper selection of antennas, and finally appropriate data acquisition parameters. The data for all three bridges were acquired using a 1.5GHz GSSI antenna with constant parameter settings as follows:

Scan/unit: 24 (scans/in)

Sample/scan: 512

Rate: 100 (KHz)

Dielectric: 7 (F/m)

# of Gain points: 1

4.2.1. Scan/Unit. This parameter defines the number of measurements taken per unit of horizontal distance. The scans per unit parameter determine the interval of horizontal sampling along the ground which is controlled by the GPR survey wheel (SIR-2 manual, 1996). A larger scans/unit value increases the number of times the ground is scanned per unit distance, returning high resolution data but large data files. This parameter is controlled by the size of the object to resolved; in this case rebar diameter controlled this parameter (Figure 4.3).

4.2.2. Rate. This is the number of scans to be stored in the system random access memory (RAM) per second. This parameter controls the speed at which the data is acquired when collecting data based on distance with a survey wheel.

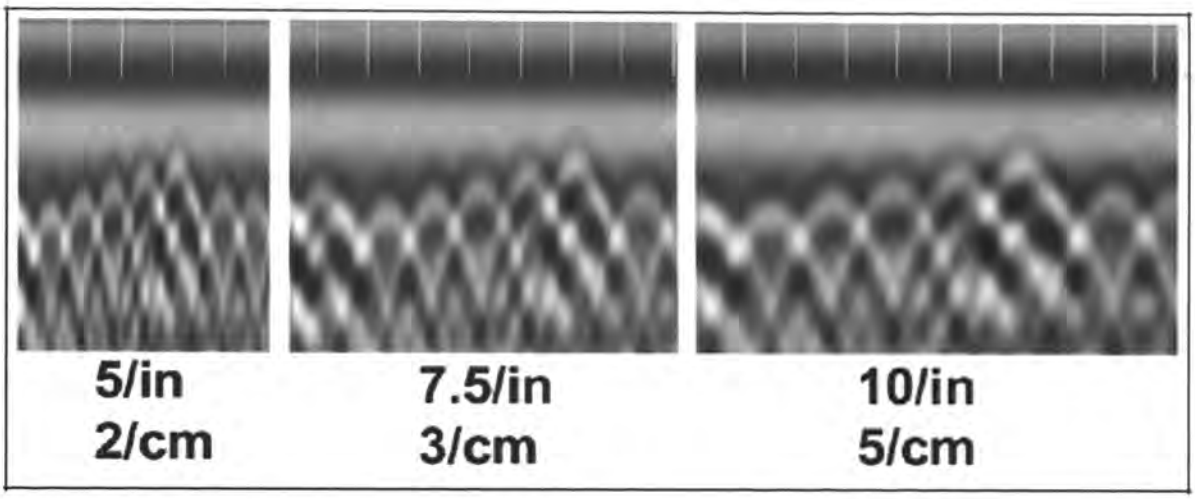

Figure 4.3 Scan spacing effects. 5 scans/in, 7.5 scans/in (optimal), and 10 scans/in settings and corresponding images for 6" wire mesh (GSSI MN72-367 Rev D, 2006).

4.2.3. Sample. A scan curve is composed of a number of individual data points (attributes of time and reflection amplitude) called samples; the more samples collected the smoother and better defined the curve will be (GSSI MN72-433 Rev F, 2006). Although more samples improve vertical resolution, as the number of scans increases the scan rate and the speed of data acquisition drops, the file size increases (GSSI MN72-433 Rev F, 2006).

4.2.4. Position. This parameter determines the beginning of the time range, generally called Time-Zero. Position is not critical during data acquisition because it can be adjusted during data processing as long as all other parameters remain constant for data comparison.

4.2.5. Range. Range is a time value in nanoseconds that defines how far the signal will penetrate into the surface. The time range is proportional to depth viewed because a longer range will allow more time for the energy to penetrate and thus provide reflections from a greater depth (GSSI MN72-433 Rev F, 2006). Range tells the system how long to record, range setting beyond the antenna penetration depth or noise floor will yield no results.

4.2.6. Gain. This is the artificial amplification of signal in order to counteract the natural effects of attenuation (GSSI MN72-433 Rev F, 2006). Attenuation of GPR signal increases with depth since some energy is reflected or absorbed. The gain function is used to boost (or amplify) the deeper (i.e., lower signal zone) signal to enhance visibility of subtle variation in weaker data. Gain ensures that the desired range is reached with an appropriately amplified pulse. Caution should be used when setting gain because too much gain on a single point will create data layer not necessarily indicative of subsurface features and can therefore cause misinterpretation (GSSI MN72-433 Rev F, 2006).

4.2.7. Stacking. This frequency noise reduction technique smooth high frequency targets and accentuates low frequency horizontal features (GSSI MN72-433 Rev F, 2006) by averaging several input scans into a single output scan. Stacking is not generally recommended in NDT, if a larger stack value is used, high frequency targets might be filtered out (Kim, 2003; GSSI MN72-433 Rev F, 2006). A high stack value also slows down data collection speed due to extra calculations involved.

4.3. DATA COLLECTION

4.3.1. GPR Data. Data acquisition with a 15GHz ground-coupled antenna is slower than with air-launched horn antennas. Earlier versions of GPR equipment required three operators: one to drive the vehicle carrying the control unit, another to control the GPR unit, and a third to drag the antenna. This project, however, required only one operator, since the new GSSI SIR System-3000 GPR unit is compact and mounted on a light push cart, one wheel of the cart functions as a survey wheel (Figure 4.4). The survey wheel is calibrated to ensure accurate measurement of the horizontal distance and accurate references for marks on the data. The direction in which GPR data is collected depends on the orientation of the top rebar mat. Typically, the data is collected in the direction perpendicular to the orientation of the top rebar mat. Design plans for all three bridges indicated that the top rebar mat was in the transverse orientation; however, this was quickly confirmed by a scan of the decks in both directions and comparison of the arrival times of both targets.

Table 4.1 describes the three bridges used in this study, showing the profiles, and cores and providing a brief overview of the deck condition. Eleven GPR profiles were acquired along separate parallel traverses across Bridge B-90-0087. The traverses were approximately 176 ft long with 2 ft spacing between adjacent traverses. A total of thirty-nine GPR profiles were acquired along separate parallel traverses on Bridge B-90-0085. Twenty profiles were used to generate contour maps of westbound Bridge C-048-0011 and, nineteen were used for eastbound Bridge C-048-0012. On westbound Bridge C-048-0011, the traverses were spaced at 2 ft interval except for traverses 19 and 20 which were only 1ft apart. Traverse spacing on eastbound Bridge C-048-0012 was 2 ft, except for

traverse 18 and 19 which were 1.5 ft apart. On Bridge A- 090-0095, a total of twenty-five GPR profiles were acquired. The traverses were approximately 286 ft long and were acquired along separate parallel traverses across the westbound (12) and eastbound (13).

Figure 4.4. GSSI SIR-3000 GPR unit equipped with 1.5GHz antenna.

4.3.2. Core Samples. Core controls were acquired from all three bridges for chloride ion content analysis, and the results were used to compare and verify the GPR data. A reinforcing steel locating device was used to locate the rebar before drilling to ensure that the rebar did not damage the core barrel and that the cores were drilled next to the rebar. Chlorides in unreinforced concrete do not cause any deterioration, therefore, testing in reinforced concrete must be performed in the area immediately surrounding the reinforcing steel (Vector Corrosion Technologies website). A 4.0 inch core barrel was used to obtain nineteen samples, eight from Bridge A-090-0095 (west- and eastbound), four from Bridge B-90-0087 (north- and southbound), and seven from Bridge C-(three from 048-0011 westbound and, four form 048-0012 eastbound) (Table 4.1). Ten of these cores were tested for chloride ion content analysis. Corrosion of rebar occurs when chloride ion content adjacent to the rebar reaches a threshold of approximately 0.025% to 0.033% by weight of concrete (or 250ppm to 330ppm) (Sohanghpurwala, 2006). The most widely applied corrosion threshold is 0.033% Cl^- by weight (2.1 lbs/y^3) of concrete, a level determined by work conducted in FHWA laboratories (Clemeña and Apusen, 2002). However, chloride threshold value remains a matter of debate. Due in part to the difficulty of determining the precise real-time state of the rebar surface and the adhesive along the interface between the rebar and the concrete (Maruya *et al.*, 2003).

Table 4.1. Summary of bridges, profiles, and cores with brief overview of decks condition.

	YEAR BUILT	ORIENTATIION	NO: LANES	BRIDGE LENGTH	PROFILES DIRECTION	NO: PROFILES	CORE SAMPLES	OVERAL BRIDGE CONDITION
BRIDGE A 090-0095	1971	Westbound	1	286 ft	E - W	12	4	Numerous severe potholes andcracks, lots of sealing and patching work on the asphalt overlay.
		Eastbound	1			13	4	
BRIDGE B 090-0087	1932 and reconstructed in 1979	Northbound	1	176 ft	N - S	11	2	Transverse cracking , mortar removal and numerous small patches.
		Southbound	1				2	
BRIDGE C 048-0011 and 048-0012	1965	Westbound	2	109 ft	W - E	19	3	Few transverse cracks and patch work.
		Eastbound	2		W - E	19	4	

4.4. DATA PROCESSING

4.4.1. GPR Data. Sometimes the problem posed, such as locating rebar in concrete can be solved by just examining the raw GPR data in the field. The 1.5GHz antenna is accurate enough to distinguish interfaces (e.g., concrete/asphalt) and determine arrival times with no data processing. Figure 4.5, for example clearly shows; the air/concrete and concrete/asphalt interface, rebar locations, suspect delaminated areas, the expansion joint and, the bottom of the bridge deck. However, very thin layers or internal concrete flaws require signal processing in order to eradicate noise that might cause misinterpretation.

Following data acquisition, the individual GPR profiles were processed using GSSI RADAN 6.5 bridge assessment module. The quality of the raw data did not require advanced processing techniques such as complex filtering and migration. The minimal processing included resizing the data files, deconvolution, time-zero correction, automated rebar reflection-picking, and analysis of the contour maps generated.

Data files were to their correct horizontal distance with reference to the bridge starting and ending joints. The start and end of a bridge can also be indicated by making marks on the data at the point when the center of the antenna coincides with the start or end of bridge.

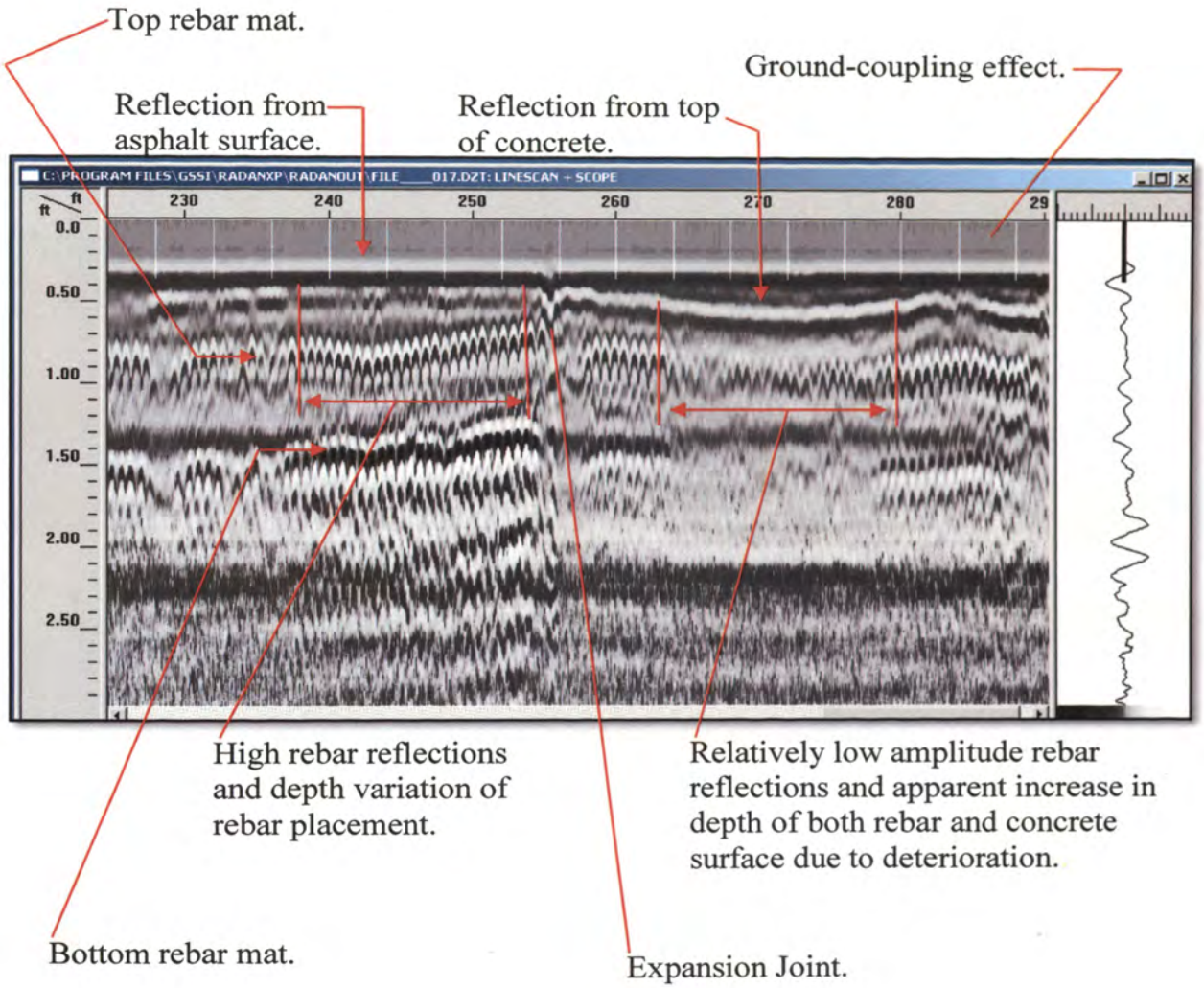

Figure 4.5. Visual examination of a GPR profile from Bridge A-090-0095.

Deconvolution was performed on all data sets to remove multiples caused by reverberation of radar energy since the multiples can cause misinterpretation. Some of the EM waves are reflected at multiple interfaces before returning to the receiver. Multiples can be classified as either long path or short path (Webb, 2000). Long path multiples have a travel path much longer than primary reflections from the same depth interfaces, hence they appear as separate events in the data. Short path multiples arrive immediately after the primary reflection, causing a change in the shape of the primary reflection (Webb, 2000). Figure 4.6 shows the difference in the data: the top image is before deconvolution, and the bottom image is after deconvolution.

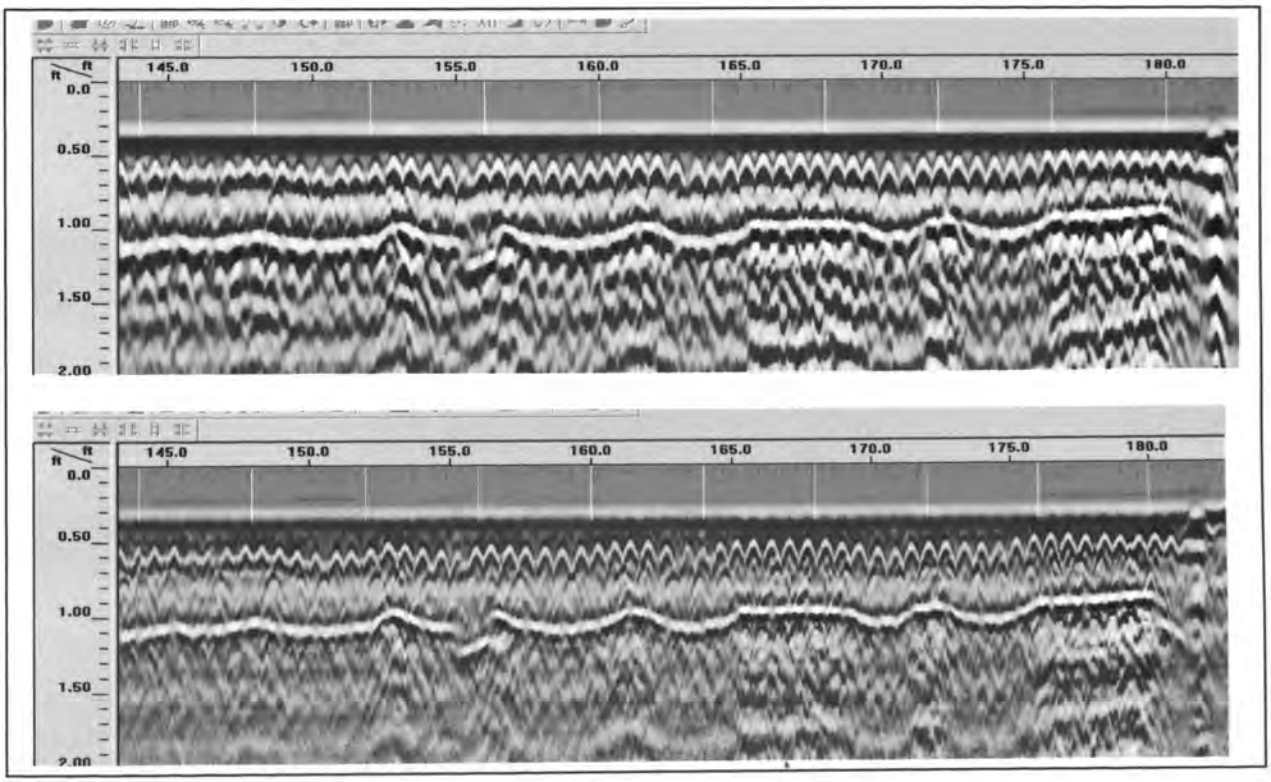

Figure 4.6. Line 4 Bridge A-090-0095 before and after deconvolution.

Time-zero correction was performed to shift each scan to correspond to the surface of the bridge deck to get the correct arrival times and accurate depth of each reflector. The time difference is primarily due to the air space between the antenna and the bridge surface. Since they include the air space, therefore, the distance and arrival times are not accurate. In Figure 4.7, the top image shows greater depth on the y-axis before time-zero correction, upward shift is apparent on the bottom image of the reflectors (about 0.2 ft) after time-zero adjustment.

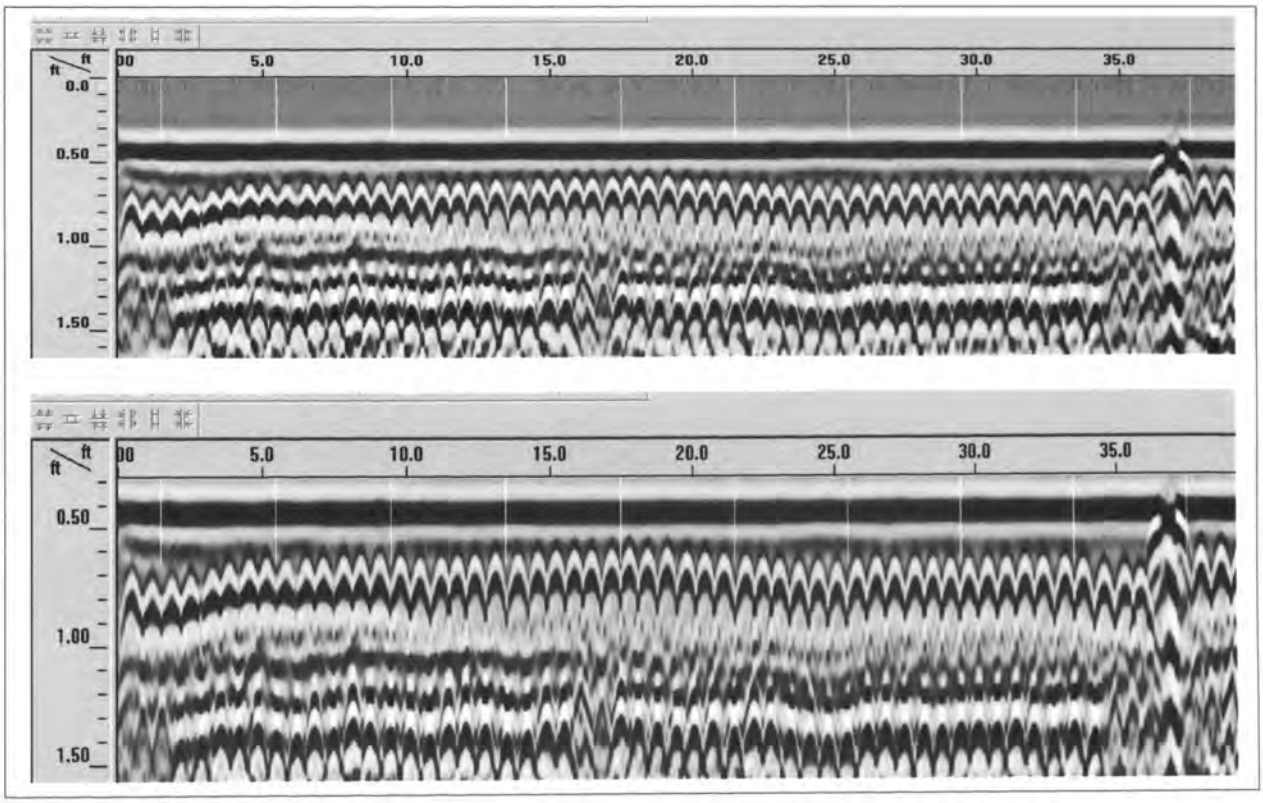

Figure 4.7. Before and after time-zero correction of data, line 2 Bridge A-090-0095.

The interactive interpretation module in RADAN 6.5 was used to automatically pick rebar reflection. Each pick is identified by a small circle on top of the data (in this case rebar) in the top interactive window pane and by a small circle located at the proper depth in the bottom window (Figure 4.8). During processing, the module displays an editable Excel spread sheet (Figure 4.8). The final product of the automated rebar picking is an ASCII database file containing the location (X and Y coordinates), depth, arrival time, and amplitude of each rebar reflection detected along the GPR profile. However, some rebar picks had to be edited or imputed because the automated picking system is not accurate in areas of severe deterioration where the rebar appear to be missing due to weak reflection (Figure 4.9).

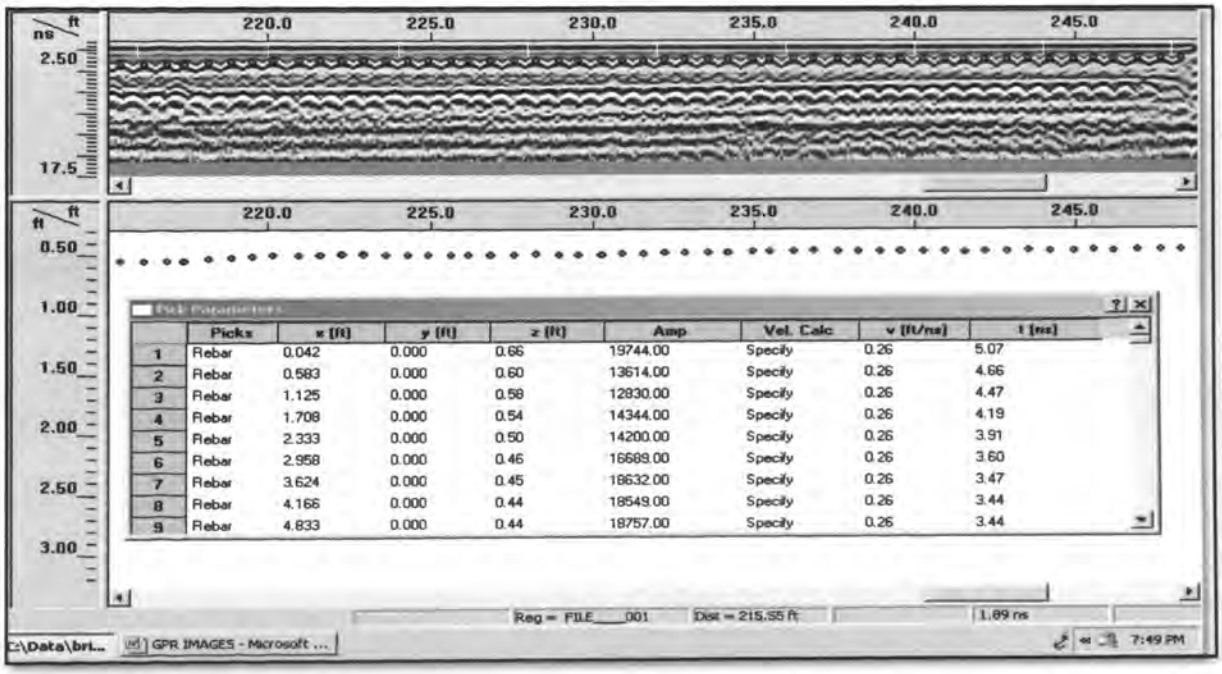

Figure 4.8. Automated rebar picking and an editable excel data table.

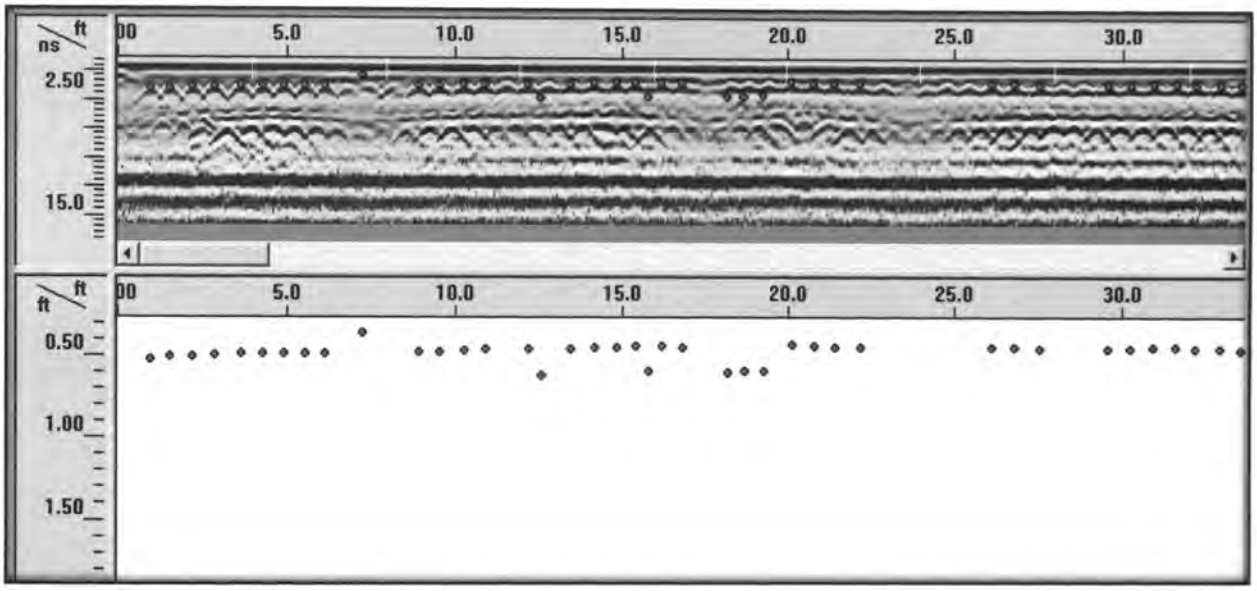

Figure 4.9. Problems with automated rebar picking on deteriorated areas with weak rebar reflection.

Surfer mapping software was used to generate contour maps using the ASCII file. Amplitude maps were created with X and Y coordinates of rebar locations and reflection amplitudes. Depth maps were generated with X and Y coordinates of rebar location and depth. A total of five amplitude maps and five depth maps were generated, including two for Bridge A-090-0095 (west- and eastbound), one for Bridge B-90-0087 (north- and southbound), and two for Bridge C-((048-0011westbound) and (048-0012-eastbound)). Figures 4.10 and 4.11 are examples of amplitude and depth maps respectively.

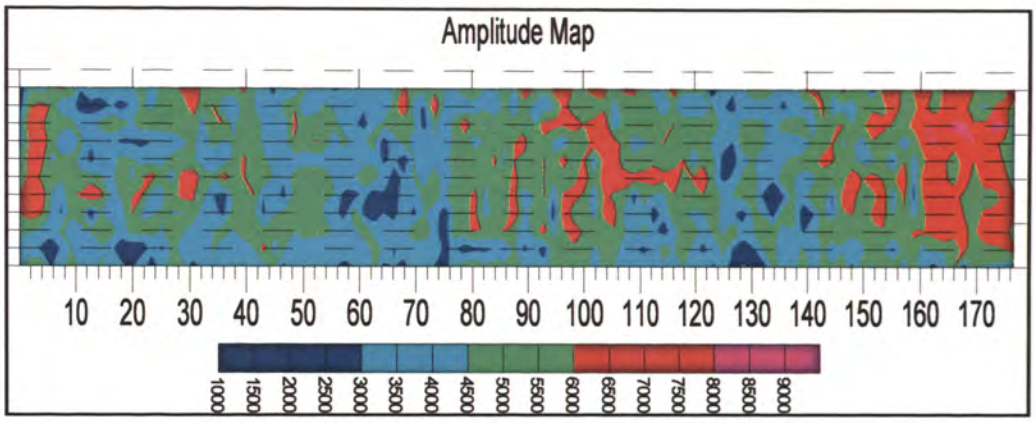

Figure 4.10. Contoured map showing variations in relative amplitudes of reflections from top of rebar of eleven GPR profiles acquired across the deck of structure No. 090-0087. Rebar amplitude increases from blue to purple.

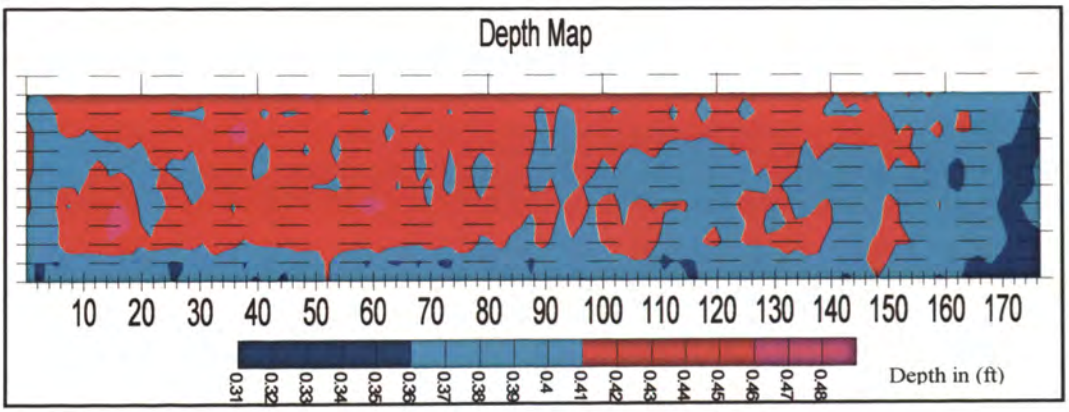

Figure 4.11. Contoured map showing variations in estimated depth (ft) of rebar on eleven GPR profiles acquired across deck of Structure No. 090-0087. Depth increases from blue to purple.

4.4.2. Chloride Ion Data. Chloride ion concentration analysis was performed by the America Petrographic Services, Inc. Chloride ion analysis was performed according to the AASHTO T 260 standard method of test for sampling and testing for chloride ion in concrete and concrete raw materials. Two powdered samples of each core between the depths of 0.25"-1.00" and 2.75"-350" were analyzed to determine chloride content and ingress. The chloride content was reported in parts per million (ppm), chloride ions per unit weight of cement (lb/yd^3), and percentage. According to the chloride ion report by the America Petrographic Services, chloride ion levels in excess of 300 to 400ppm corrode reinforcing steel in concrete and significantly increase the number of freeze-thaw cycles. Additionally, de-icing salt allow the concrete to become critically saturated increasing the severity of each freeze-thaw cycle. The unit weight of concrete on the three bridges was between 4000 and 4020 lb, and the following formulas were used to generate chloride ion values:

$$Cl^{-}lbs/yd^3 = \frac{ppm}{10^6} \times Unit\ Weight\ of\ concrete\ (lbs) \quad (4.1)$$

$$\%Cl^{-} = \frac{ppm}{10^6} \times 100 \quad (4.2)$$

4.5. DATA ANALYSIS AND INTERPRETATION

In the preliminary phase of data interpretation, the unprocessed GPR data was examined visually. In general, depending on the level of deterioration, problem zones within the bridge deck can be identified by rebar image reflection magnitudes and arrival times. In Figure 4.12a, areas of intact rebar and concrete are characterized by laterally continuous rebar reflections/diffractions of uniformly high magnitude with relatively short arrival times. In contrast, areas of possible extensive delamination are characterized by lower magnitude reflections/diffractions with greater arrival times (Figure 4.12b). However, due to discrepancies between design plan and actual rebar placement determination of deterioration by travel times can be inaccurate. Similarly, signal magnitudes can vary because of factors (e.g., the presence of a mud layer) other than the presence of delaminations.

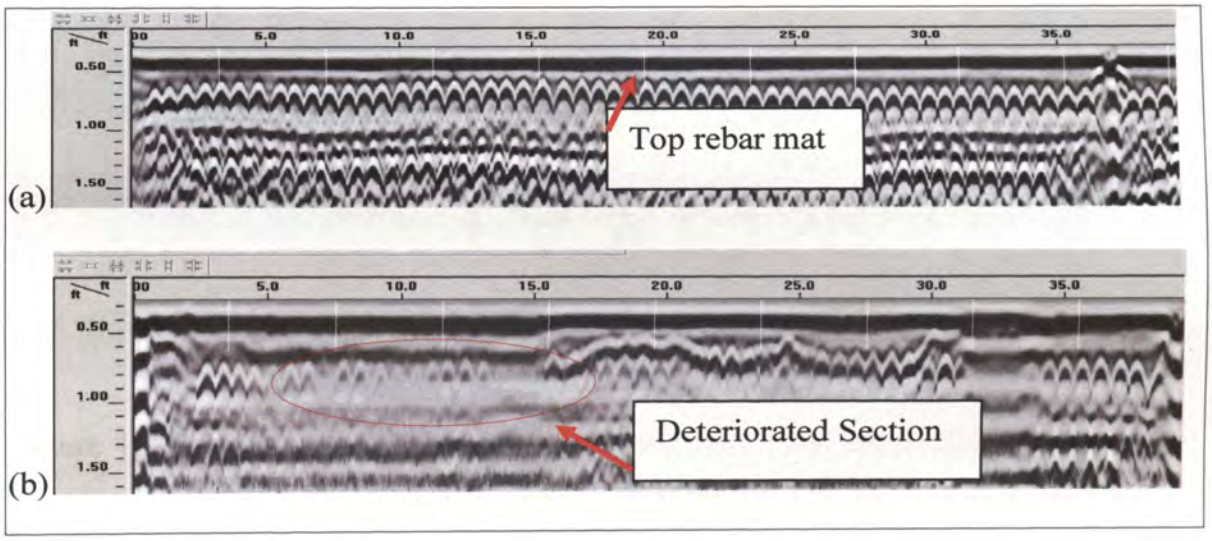

Figure 4.12. Examples from Bridge A-090-0095: (A) consistent signature for top rebar mat; (B) signature displaying amplitude and travel-time anomalies distinguishing areas of possible deterioration.

Careful analysis of the depth maps of all three bridges, demonstrated that these maps did not accurately indicate delamination. This conclusion is based on three observations of significant depth variation due to inconsistent rebar placement. Profile (2) of Bridge A-090-0095 shows variation in rebar depth in a profile that does not show any signs of delamination (Figure 4.13). Profile (1) of Bridge B-90-0087 and profile (11) of Bridge C-048-0012 show alternating depth variation within the same profile (Figure 4.14 (a) and (b) respectively). Poor workmanship and inadequate documentation of both original and repair work data complicated the determination rebar placement and patches with asphalt overlay.

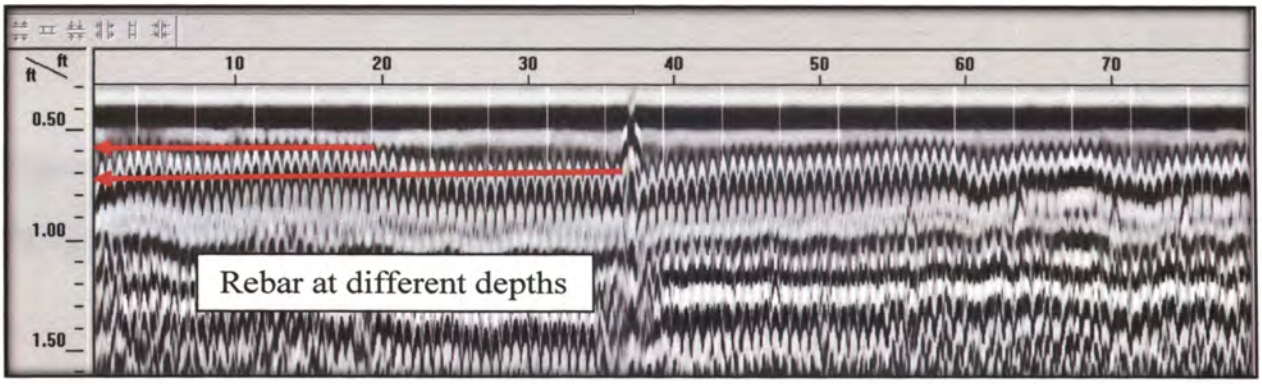

Figure 4.13. Depth variation due to inconsistent rebar placement (design flaw).

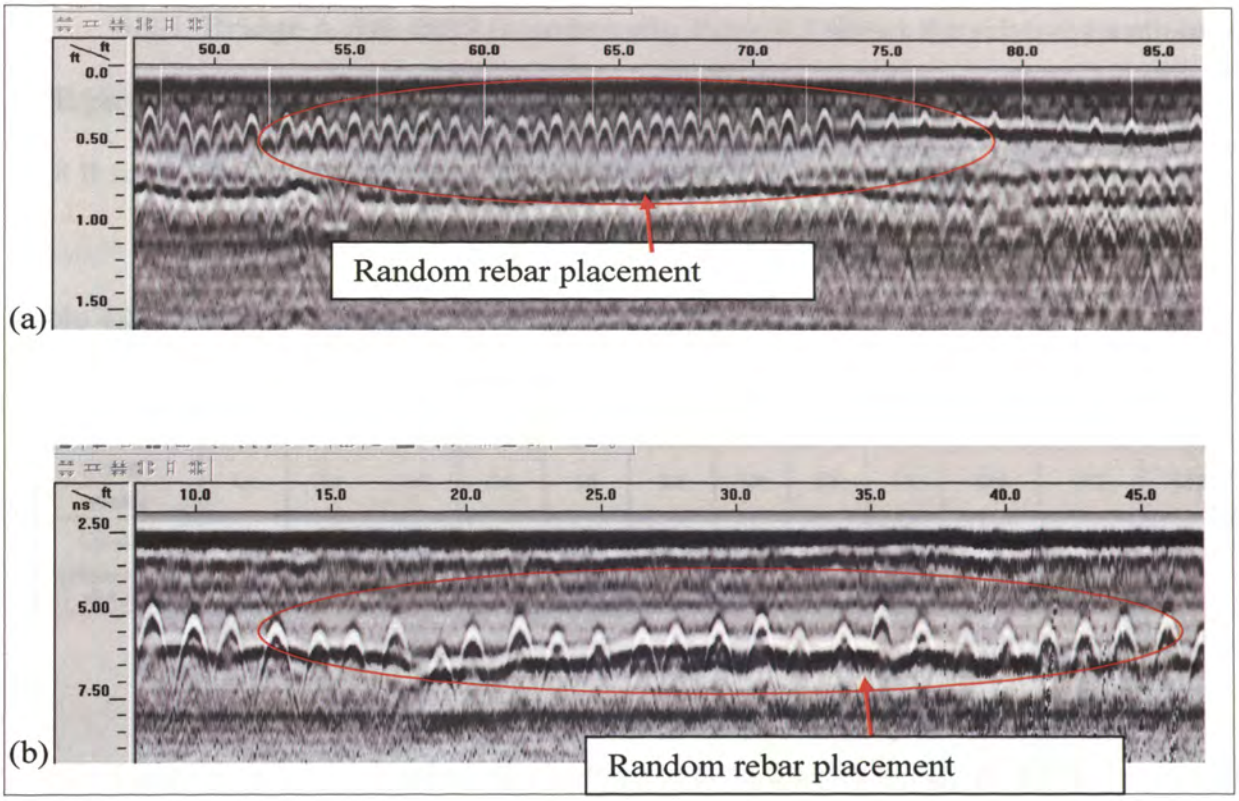

Figure 4.14. Variation due to random inconsistent rebar placement. (A) Example from Bridge B-90-0087, and (B) Example from Bridge C-048-0011.

On the amplitude maps, zones with a high probability of deterioration or delamination were identified on the basis of reflection magnitude obtained from the automatic rebar-picking tool. On the amplitude maps deep blue areas were interpreted as likely areas of significant deterioration; light blue areas were interpreted as probable deterioration.

4.5.1. Bridge A-090-0095 (westbound). Table 4.2 shows the relative locations of GPR profiles acquired on the westbound (left) lanes. Traverse L1 and L12 are 1.5 ft and 21.8 ft south of the northern edge of the westbound lane, respectively.

Table 4.2. Location of GPR profiles acquired in the westbound (left) lane

GPR Profile	L1	L2	L3	L4	L5	L6	L7	L8	L9	L10	L11	L12
Location (Figure 4.15 & 4.16)	20.3	18.3	16.3	14.3	12.8	11.8	10	8	6	4	2	0

Core control was acquired at four locations on this deck (Figure 4.15). Table 4.3 summarizes field and laboratory observations based on these cores. Their locations are also superimposed on the amplitude map (Figure 4.16). Field examination of the four cores (Table 4.3) shows deterioration of concrete, asphalt or both. Deep blue areas (<5000 relative rebar reflection) on the amplitude map (Figure 4.16) indicate significant deterioration and/or high chloride ion content (above 400ppm). Light blue areas probably indicate deterioration and/or elevated chloride ion content (>5000 <7000).

Table 4.4 is a summary of chloride ion concentration. Cores C-1 and C-4 were taken from that part of the bridge that appeared most deteriorated (south section of westbound) (Figure 4.15). This deterioration is due to poor design; the lanes are banked south toward the median with no water outlets, permitting the accumulation of debris and stagnant water (Figure 4.15). The chloride ion concentration in cores C-1 and C-4 was far beyond the threshold of 400ppm at which corrosion of reinforcing rebar is expected

(Table 4.4). The top part of each core (0.25"-1.00") had high chloride ions concentration than the deeper (2.75"-3.50") potion of the core, indicating that the deterioration concentrated on the top part of the bridge deck may be as a result of de-icing salt. The chloride ions concentration (Table 4.4) correlates well with the field observations (Figure 4.15; Table 4.3) and the amplitude map (Figure 4.16).

Figure 4.15. Part of the most (visually) deteriorated part of Bridge A-090-0095 (westbound).

Table 4.3. Summary of core control acquired on Bridge A-090-0095 (westbound lanes). Core locations are superposed on Figure 4.16.

BRIDGE A - 090-0095 (Westbound)									
SCI Core No.	Data Cored	Location - Stationing, GPR Line Survey, and Lane Designation			Average (inches) Core Length		Chloride Ion Content in PPM (Cl lbs/CY)	Field Observation	Laboratory Observation (Photographs Included)
					Asphalt	Concrete			
C-1	3/11/2008	28+83	L12	Lt.	2	3.7	Refer to APS Report - April 17, 2007	Asphaltic concrete appeared deteriorated. Top 2 inches of concrete cored easily and top 1 inch of concrete crumbled.	Asphalt core not intact and asphalt thickness determined in the field is reported. Reinforcing bar not observed in core.
C - 2	3/11/2008	28+86	L5	Lt.	1.4	7	-	Cored in newer concrete/patch area. Asphaltic concrete appeared deteriorated. The concrete core did not appear delaminated.	Asphalt core and concrete core are one unit (total 8.2 inches). Asphalt core length measured at approximately 1.3 to 1.5 inches with average reported. Reinforcing bar not observed in core.
C-3	3/11/2008	29+88	L8	Lt.	1.3	5.3	-	Top 1 to 2 inches of asphaltic concrete appeared deteriorated.	Reinforcing bar at base of concrete core.
C-4	3/11/2008	30+34	L12	Lt.	2	4.6	Refer to APS Report - April 17, 2007	Asphaltic concrete appeared deteriorated.	Asphalt core not intact and asphalt thickness determined in the field is reported. Concrete core fragmently slightly - top and bottom of core could not be determined.
		TOTAL AVERAGE			1.7	5.2			

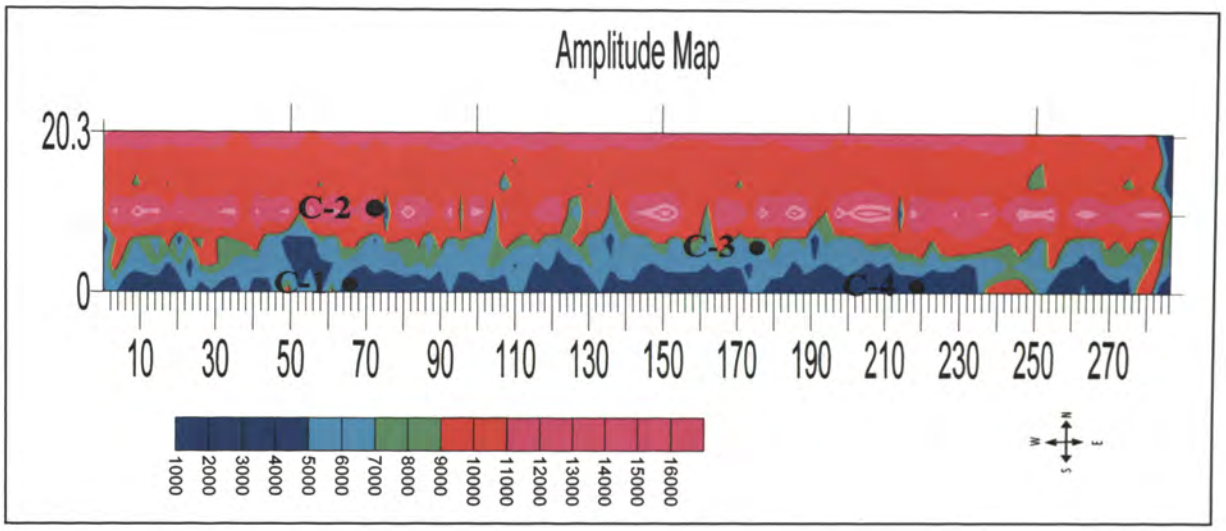

Figure 4.16. Contoured map showing variations in the relative amplitudes of reflections from top of rebar on GPR profiles and superimposed core locations acquired across westbound lanes of Bridge A-090-0095.

Table 4.4. Summary of chloride ion concentration data acquired at Bridge A-090-0095 (westbound lanes).

CHLORIDE ION CONTENT BRIDGE A-090-0095 (Westbound)			
Sample Number	Parts Per Million	Cl^- lbs/yd^{3**}	%Cl^-
C-1 (0.25"-1.00")	>6000	>24.0	>0.60
C-1 (2.75"- 3.50")	990	4	0.1
C-4 (0.25"-1.00")	4015	16.2	0.4
C-4 (2.75"- 3.50")	1085	4.4	0.11

4.5.2 Bridge A-090-0095 (eastbound). Table 4.5 shows the relative locations of GPR profiles acquired on the eastbound (right) lanes of Bridge A-090-0095. Traverses R13 and R1 are 2 ft and 22.4 ft south of the northern edge of the eastbound lane, respectively.

Table 4.5. Location of GPR profiles acquired in the eastbound (right) lane.

GPR Profile	R1	R2	R3	R4	R5	R6	R7	R8	R9	R10	R11	R12	R13
Location (Figure 4.17)	0	1	2	4	6	7.5	8.4	10.4	12.4	14.4	16.4	18.4	20.4

Core controls were acquired at four locations, as shown in Figure 4.17. Field observation (Table 4.6) of core C-5 showed asphalt deterioration and concrete delamination, cores C-6, C-7, and C-8 show concrete delamination. Chloride ion analysis (Table 4.7) was carried out on cores C-5 and C-8, showing levels of chloride ions beyond both the corrosion threshold of 400ppm (0.04%) established by American Petrographic Services and that of or 0.033% used by the FHWA. In the westbound lanes, most deterioration was concentrated in the south section, but the eastbound amplitude map shows a more widespread deterioration and or delamination. Although the eastbound lanes of this bridge appear to be in excellent condition, the chloride ions at depths of 0.25"-1.00" is significantly higher than at the same depth in the south section of westbound lanes which appear severe deteriorated. These discrepancies between surface appearance and chloride ion content indicates that although visual inspection can help to determine an initial cause of action, they are not a reliable basis of discussion regarding concrete remediation. Deep

blue areas on the amplitude map (Figure 4.17) indicate significant deterioration and high chloride ion content (<5000 rebar amplitude and >400ppm); Light blue areas probably indicate deterioration and/or elevated chloride ion content (>5000 <7000 amplitudes).

Table 4.6. Summary of core control acquired on Bridge B-090-0095. Core locations are superposed on Figure 4.17.

BRIDGE A - 090-0095 (Easttbound)									
SCI Core No.	Data Cored	Location - Stationing, GPR Line Survey, and Lane Designation			Average (inches) Core Length		Chloride Ion Content in PPM (Cl lbs/CY)	Field Observation	Laboratory Observation (Photographs Included)
					Asphalt	Concrete			
C-5	3/11/2008	28+87	L7	Rt.	1.3	6.3	Refer to APS Report - April 17, 2007	Asphaltic concrete deteriorated. Top 1 inch of concrete appeared delaminated.	Asphalt core not intact and asphalt thickness determined in the field is reported. Top of concrete core appears fragmented. Reinforcing bar present with no visible indication of corrosion. Imprint of rebar observed at base of core.
C-6	3/11/2008	29+53	L11	Rt.	2.2	4.9	–	Appeared deteriorated around top mat of reinforcing rod.	Corrosion observed around the top reinforcing bar. Imprint of reinforcing bar observed at base of core.
C-7	3/11/2008	30+11	L8	Rt.	2.2	5.4	–	Top 1/2 inch of concrete deteriorated.	Asphalt core and concrete core are one unit (total 7.8 inches). Asphalt core length measured at approximately 2 to 2.4 inches with average reported. Reinforcing bar at base of concrete core.
C-8	3/11/2008	30+70	L3	Rt.	1.4	4	Refer to APS Report - April 17, 2007	Top 1 to 1.5 inches of concrete appeared delaminated and crumbled.	Reinforcing bar not observed in core.
		TOTAL AVERAGE			1.8	5.2			

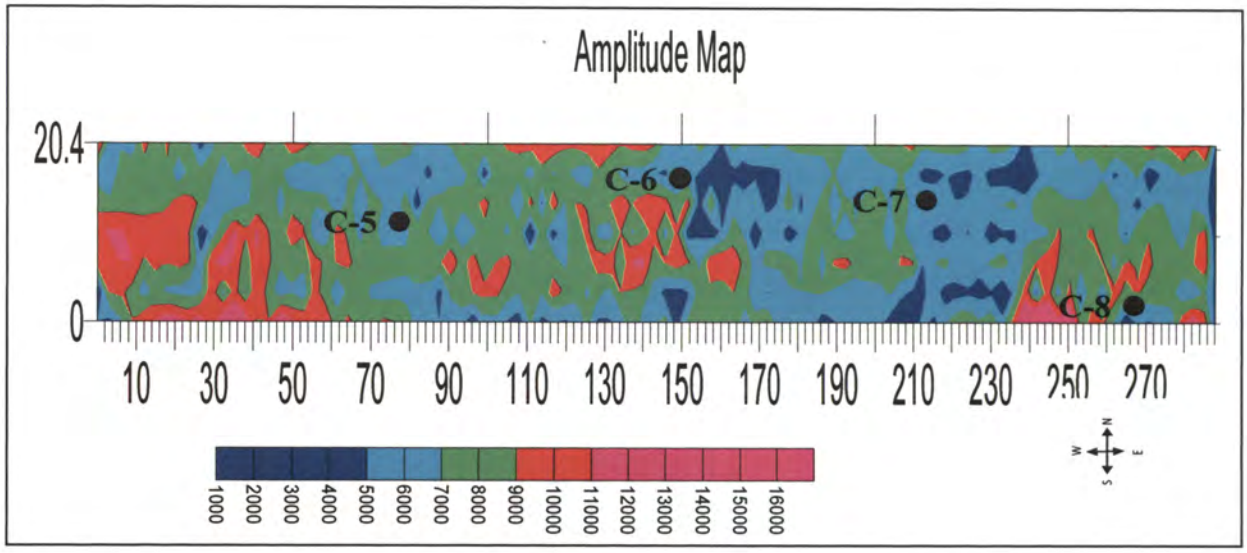

Figure 4.17. Contoured map showing variations in relative amplitudes of reflections from top of rebar on GPR profiles and superimposed core locations acquired across eastbound lanes of Bridge A-090-0095.

Table 4.7. Summary of chloride ion concentration data acquired at Bridge A-090-0095 (eastbound lanes).

CHLORIDE ION CONTENT BRIDGE A-090-0095 (Eastbound)			
Sample Number	Parts Per Million	Cl^- lbs/yd^{3**}	%Cl^-
C-5 (0.25"-1.00")	5190	20.9	0.52
C-5 (2.75"- 3.50")	3780	15.2	0.38
C-8 (0.25"-1.00")	4700	18.9	0.47
C-8 (2.75"- 3.50")	2535	10.2	0.25

4.5.3. Bridge B-090-0087. This was the only bridge without asphalt overlay. A total of eleven GPR profiles were acquired along separate parallel traverses across the deck. The eastern-most GPR traverse (1) was 2 ft from the outer edge of the lane. The spacing between adjacent traverses was 2 ft (Figure 4.18). Table 4.8 is a summary of four cores samples with their locations superimposed on Figure 4.18. Deep blue areas on the amplitude map indicate significant deterioration and high chloride ion content (<3000 rebar amplitude and >400ppm); Light blue areas probably indicate deterioration and/or elevated chloride ion content (>3000 <4500 amplitudes).

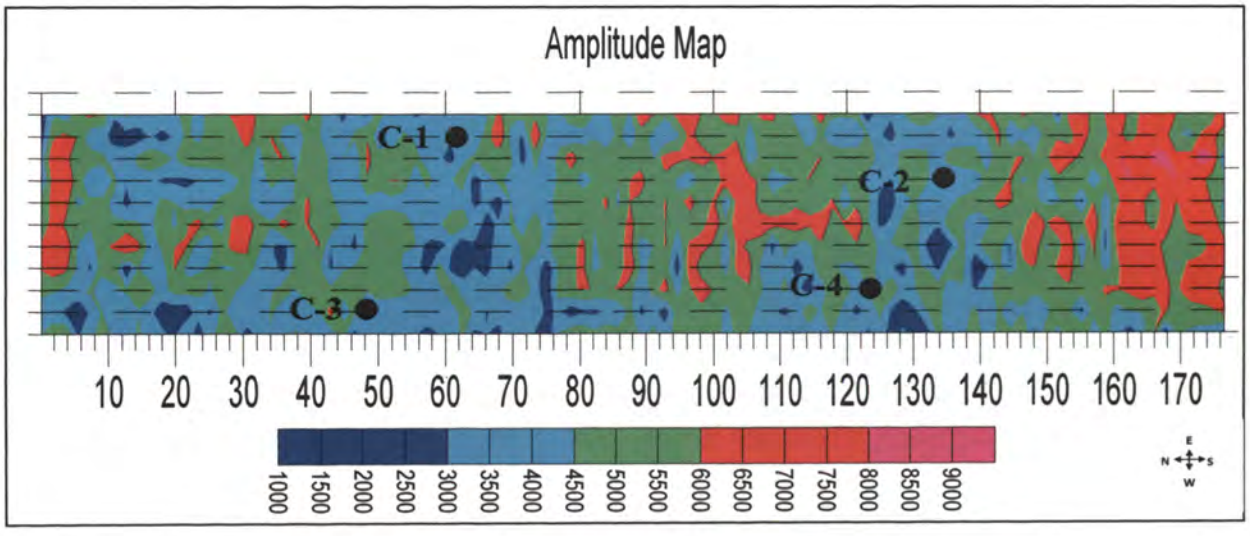

Figure 4.18. Contoured map showing variations in relative amplitudes of reflections from top of rebar acquired across deck of Bridge B-090-0087, with core locations superposed.

Table 4.8. Summary of core control acquired on Bridge B-090-0087. Core locations are superposed on Figure 4.18.

Bridge B-090-0087									
Core No.	Data Cored	Location - Stationing, GPR Line Survey, and Lane Designation			Average (inches) Core Length		Chloride Ion Content in PPM (Cl lbs/CY)	Field Observation	Laboratory Observation
					Asphalt	Concrete			
C-1	3/12/2008	4+32	L2	Lt.	N/A	8.1	Refer to chloride-ion content table	Cored 7 inches - could not retrieve bottom portion of core. Core appeared delaminated in top 2 to 3 inches of core. Core fractured in 2 pieces.	Reinforcing bar not observed in core. Fracture visible in upper portion of core.
C-2	3/12/2008	5+00	L4	Lt.	N/A	5.7	–	Solid core, however appeared delaminated.	Corrosion observed around the reinforcing bars. Delamination appears present within the core.
C-3	3/12/2008	4+17	L10	Rt.	N/A	4.7	–	Top 1 to 2 inches and bottom 4 inches of core appeared deteriorated. Photograph obtained of core hole.	Reinforcing bar not observed in core.
C-4	3/12/2008	4+90	L9	Rt.	N/A	5.9	Refer to chloride-ion content table	Top 1 to 3 inches of core appeared deteriorated.	Reinforcing bar not observed in core.
		TOTAL AVERAGE			N/A	6.1			

Table 4.9 shows that the chloride ion concentration decreases with depth and is highest in the upper 0.25"-1.00". Core C-1 shows significantly lower chloride ion concentration at depths of 2.75"- 3.50". These levels indicate that ingress at this section is not high although the core hole (Figure 4.19) clearly shows delamination. In Figure 4.20, cracks can be seen propagating the whole length of core. This indicates that part of the bridge deck seriously damaged. The chloride ion concentration correlates well with the amplitude map and indicates that the top 0.25"-1.00" of the bridge deck needs rehabilitation.

Table 4.9. Summary of chloride ion concentration data acquired at Bridge A-090-0087.

CHLORIDE ION CONTENT BRIDGE B-090-0087 (North and Southbound)			
Sample Number	Parts Per Million	Cl^- lbs/yd^{3**}	%Cl^-
C-1 (0.25"-1.00")	3525	14.2	0.35
C-1 (2.75"- 3.50")	170	0.7	0.02
C-4 (0.25"-1.00")	3685	14.8	0.37
C-4 (2.75"- 3.50")	2010	8.1	0.2

Figure 4.19. Core hole showing planer separation of concrete from Bridge A-090-0087 core C-1.

Figure 4.20. Deteriorated core sample from Bridge A-090-0087 core C-2 showing cracks and voids through length of core.

4.5.4. Bridge C-048-0011 (westbound). On this deck nineteen GPR profiles were acquired along separate parallel traverses. The northern-most GPR traverse (1) was 2 ft south of the northern edge of the lane. The traverses were spaced at 2 ft intervals except for traverses 18 and 19, which were only 1ft apart (Figure 4.22). Visual inspection of the top face of the bridge deck showed no signs of deterioration. There were few cracks and repair patches; however, the underside of the bridge (Figure 4.21) revealed massive corrosion of the bottom rebar mat around the drainage outlets. This damage is as a result of inadequate drainage, outlets are just open holes without a gutter system to direct the flow away from the bridge bottom. Another design deficiency shown in Figure 4.21 is the placement of rebar at shallow depth in the concrete, making it prone to corrosion. The four cores acquired at this location are summarized in Table 4.10 and the chloride ion report on two of these cores (Table 4.11) revel that despite the damage on its underside the bridge is in good condition. The reflection amplitudes contour map in Figure 4.22 shows very few areas of deterioration, further confirming that this bridge is in good condition. The amplitude map (Figure 4.22) indicates that the overall bridge condition is good. Although core C-2 shows chloride ion levels above the corrosion threshold, this is a localized problem. Chloride ingress is also low (Table 4.22). Comparison of the results for this bridge with those for the other two indicate that the chlorides-ion concentration below 1000ppm, although well above the threshold of 400ppm this level does not significantly reduce rebar reflection amplitude.

Figure 4.21. Significant deterioration on underside of Bridge C- 048-0011 around drainage outlets.

Table 4.10. Summary of core control acquired on Bridge A-048-0011 (westbound lanes). Core locations are superposed on Figure 4.22.

BRIDGE C - 048 - 0011 (Westbound)									
Core No.	Data Cored	Location - Stationing, GPR Line Survey, and Lane Designation			Average (inches) Core Length		Chloride Ion Content in PPM (Cl lbs/CY)	Field Observation	Laboratory Observation
					Asphalt	Concrete			
C-1	3/12/2008	569+79	L2	Lt.	2	11.5	-	Cored full depth of core bit (14 inches)	Asphalt core and concrete core are one unit (13.6 inches). Asphalt core length measured at approximately 2 inches. Reinforcing bar observed in core. Corrosion or delamination not observed.
C - 2	3/12/2008	569+89	L8	Lt.	2	11.6	Refer to chloride-ion content table	Top 2 inches of concrete core appeared delaminated	Asphalt core and concrete core were measured as one unit (13.6 inches). Asphalt core length measured at approximately 2 inches. Top 2 inches of concrete core separated from bottom portion.
C-3	3/12/2008	570+32	L9	Lt.	1.5	12.3	Refer to chloride-ion content table	-	Asphalt core and concrete core are one unit (13.8 inches). Asphalt core length measured at approximately 1.5 inches. Reinforcing bar observed in the upper portion of concrete core. Corrosion or delamination not observed.
C-4	3/13/2008	569+87	L18	Rt.	1.7	7	-	Top 1 to 2 inches of core appeared delaminated and deteriorated.	Slight deterioratin observed near the top of the concrete core and concrete fragments from the upper portion of the core. Reinforcing bar not observed in core.
		TOTAL AVERAGE			1.8	10.6			

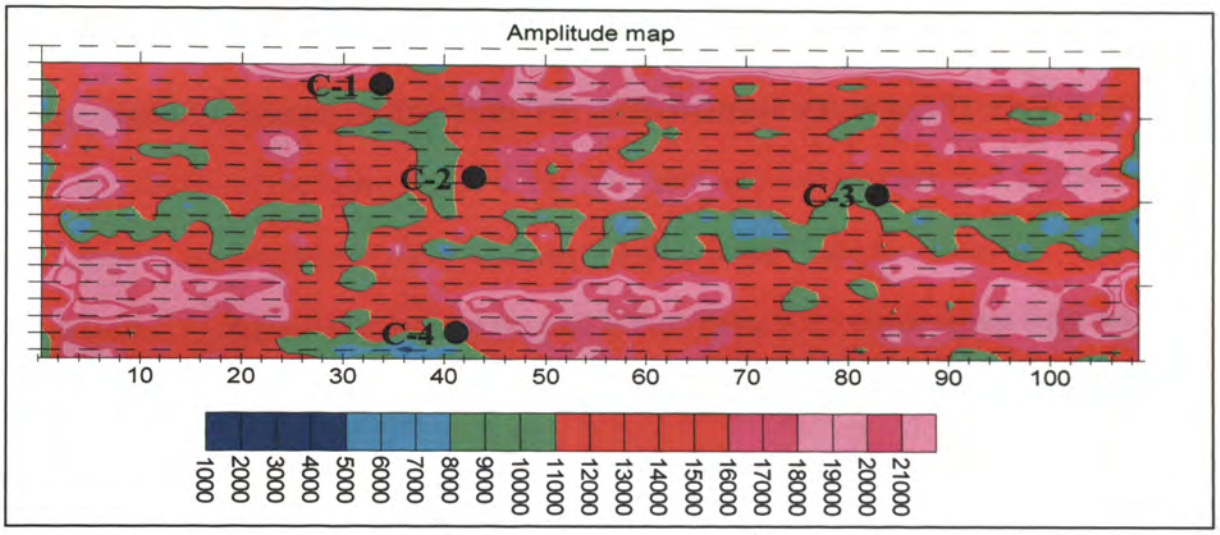

Figure 4.22. Contoured map showing variations in relative amplitudes of reflections from top of rebar on GPR profiles acquired across deck of Bridge C-048-0011 (westbound), with core locations superposed.

Table 4.11. Summary of chloride ion concentration data acquired at Bridge C-048-0011.

CHLORIDE ION CONTENT BRIDGE C-048-0011 (Westbound)			
Sample Number	Parts Per Million	Cl^- lbs/yd^{3**}	%Cl^-
C-2 (0.25"-1.00")	1025	4.1	0.1
C-2 (2.75"- 3.50")	625	2.5	0.06
C-3 (0.25"-1.00")	835	3.3	0.08
C-3 (2.75"- 3.50")	<80	<0.3	<0.01

4.5.5. Bridge C-048-0012 (eastbound). Nineteen traverses were acquired along separate parallel traverses on this deck. The northern-most traverse (19) was 2 ft south of the northern edge of the lane (Figure 4.23). The traverses were spaced at 2 ft intervals. Core control was acquired at three locations on this deck. These locations are superimposed on the amplitude map (Figure 4.23). Table 4.12 summarizes field and laboratory observations of these cores. Field examination of the three cores (Table 4.12) shows deterioration of concrete, asphalt or both. Deep blue areas (<5000 rebar amplitude) on the amplitude map (Figure 4.23) indicate of significant deterioration and high chloride ion content. Light blue areas probably indicate deterioration and elevated chloride ion content. Table 4.13 is a summary of chloride ion concentration. A significant amount of chloride ions was detected in the top 0.25"-1.00" of the cores as well as ingress to a depth of 2.75"- 3.50". However, the amplitude map the problem is not widely spread so rehabilitation work maybe sufficient.

Table 4.12. Summary of core control data acquired on Bridge A-048-0012 (eastbound lanes). Core locations are superposed on Figure 4.23.

BRIDGE C - 048-0012 (Eastbound)									
Core No.	Data Cored	Location - Stationing, GPR Line Survey, and Lane Designation			Average (inches) Core Length		Chloride Ion Content in PPM (Cl lbs/CY)	Field Observation	Laboratory Observation
					Asphalt	Concrete			
C-1	3/13/2008	570+50	L2	Rt.	1.8	9.1	Refer to chloride-ion content table	Top 1 inch of core appeared delaminated. Top 1 inch of core crumbled.	Reinforcing bar not observed in core. Corrosion or delamination not observed.
C-2	3/13/2008	569+86	L12	Lt.	0.9	6.1	-	Cored in newer concrete/patch area. Asphaltic concrete appeared deteriorated. The concrete core did not appear delaminated.	Asphalt core appeared deteriorated. Reinforcing bar, reinforcing bar imprint, and other metal observed in the concrete core. Corrosion or delamination not observed.
C-3	3/13/2008	570+63	L14	Lt.	1.4	8.8	Refer to chloride-ion content table	Top 2 inches of core appeared delaminated.	Detached reinforcing bar appeared corroded.
		TOTAL AVERAGE			1.4	8			

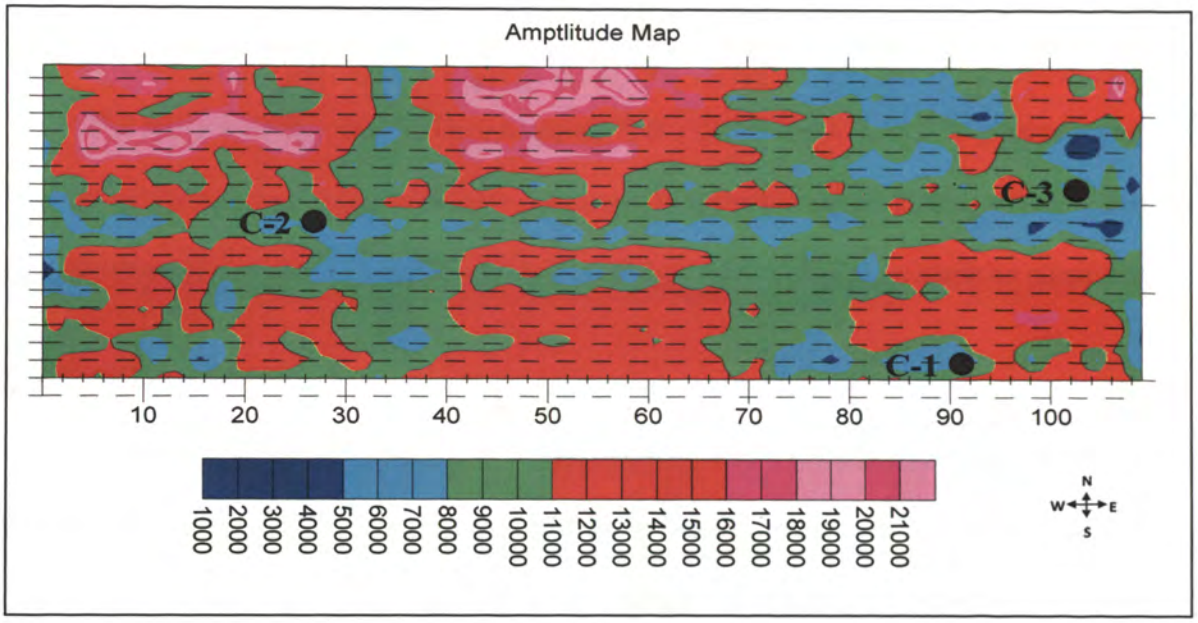

Figure 4.23. Contoured map showing variations in relative amplitudes of reflections from top of rebar on GPR profiles acquired across deck of Bridge C-048-0012 (eastbound), with core locations superposed.

Table 4.13. Summary of chloride ion concentration data acquired at Bridge C-048-0012.

CHLORIDE ION CONTENT BRIDGE C-048-0012 (Eastbound)			
Sample Number	Parts Per Million	Cl^- lbs/yd^{3**}	%Cl^-
C-1 (0.25"-1.00")	1810	7.3	0.18
C-1 (2.75"- 3.50")	1500	6	0.15
C-3 (0.25"-1.00")	>6000	>24.0	>0.60
C-3 (2.75"- 3.50")	1080	4.3	0.11

5. CONCLUSIONS AND RECOMMENDATIONS

The results of this study demonstrated that GPR with a 1.5 GHz ground-coupled antenna is effective in finding deteriorated areas in a bridge deck. It also offers a fast and cost effective alternative to traditional bridge inspection techniques such as sounding.

5.1. CONCLUSIONS

Amplitude maps, chloride ion concentration, and visual inspections were used to estimate the amount of deterioration on the three bridge decks. On the amplitude maps, the areas color coded deep and light blue are indicative of severe to mild deterioration respectively. These areas were used to estimate the percentage of deterioration on the bridges. State departments of transportation (DOTs) require action if between 5% and 20% of the total deck area is deteriorated and when chloride concentrations exceed a threshold of 2.0 lbs/yd^3 of concrete (Guthrie and Hema, 2005).

5.1.1. Bridge A-090-0087 (westbound). This bridge had severe deterioration concentrated on the southern shoulder. From the amplitude map, it is estimated that 37% of the bridge area is deteriorated. Chloride ions concentrations at depths of 3.25" in the south section of the bridge were significantly beyond the corrosion threshold of 2.0 lbs/yd^3. Recommended repair on the entire south section includes removal of dereriorated concrete and replacement of damaged rebars. Building of drainage outlets on the south shoulder will help prevent the accumulation of debris which results in stagnant water leading to potholes and increased chloride ions ingress.

5.1.2. Bridge A-090-0095(eastbound). 53% of this bridge had wide speed deterioration, chloride ions concentrations at depths of 3.25″ were greater than 2.0 lbs/yd^3. Due to spread deterioration, removal of the deteriorated concrete on the entire bridge and replacement of corroded rebars is recommended. Widening and increasing the number of drainage outlets will prevent the accumulation of mud on the south shoulder of the bridge.

5.1.3. Bridge B-090-0087. It was estimated that 54% of this bridge was deteriorated with chloride concentration significantly above the corrosion threshold of 2.0 lbs/yd^3. The deterioration is also wide spread, hence recommended rehabilitation includes stripping deteriorated concrete on the entire bridge and replacing corroded rebars.

5.1.4. Bridge C-048-0011 (westbound). Of all the three bridges, this bridge was in excellent condition. It was estimated that only about 3% of the bridge was deteriorated. Chloride ions concentrations were less than 4.2 lbs/yd^3 at depths of 3.25″ in the affected areas. The deterioration is localized, hence replacing of concrete in these areas is recommended. A gutter system is needed to redirect storm water at the drainage outlets away from the underside of the bridge.

5.1.5. Bridge C-048-0012 (eastbound). It was estimated that 18% of this bridge was deteriorated, however, the chloride ions concentrations at depths of 3.25″ were not significantly above the corrosion threshold. Rebar amplitudes on the GPR profiles did not indicate significant deterioration, therefore replacing of concrete on the affected areas is recommended.

5.2. RECOMMENDATIONS

To realize the full benefits of GPR for bridge deck assessment improvement is needed in workmanship and accountability. The lack of proper repair documentation for the three bridges in this study significantly hindered identification and understanding of the various features revealed in the GPR profiles. It is widely accepted that where there are phase (or travel time) variations, deterioration can be mapped. In fact, however, design flaws in rebar placement often make mapping impossible. It is next to impossible to engineer a bridge deck with perfectly consistent rebar depth. However this problem can be overcome by GPR. GPR profiles entered in a database immediately after bridge construction would provide a basis for comparison by documenting rebar placement. The drainage problems observed on the underside of Bridge C-048-0011 (westbound) are as a result of negligence. Since corrosion of bridge deck reinforcing rebar remains a challenge for transportation agencies, more funds are required for experimentation with various reinforcing material with the potential to increasing the deck service life and to lengthen the periods between expensive rehabilitation efforts.

Although 1.5 GHz ground-coupled antennas yielded good results, the user requires significant time and causes traffic obstruction. The focus of research should shift toward improvement of air-launched antennas that offer the advantage of faster data collection and the safety of working inside a vehicle. Using RADAN 6.5 Interactive Interpretation, the user can automatically pick peak rebar amplitudes from a GPR profile. In bridge deck assessment, these picks output only depth and amplitude values; the software is not designed to identify zones of attenuated signal that may indicate deterioration. Additional work is also required to determine what reflection amplitude

reliably indicates deterioration. With further research GPR might not only indicate a problem but also identify delamination, debonding of concrete from reinforcement, and corrosion. Visual assessment of a rebar scan can provide a rough identification of intact and deteriorated areas; however, amplitude maps and chloride ion analysis yields better accurate results. Finally performance-based specifications and measurement standards must be developed for GPR to ensure that profiles stored in the database are accurate and to permit performance evaluations. Overall GPR provides valuable data for transportation infrastructure management and rehabilitation programs.

BIBLIOGRAPHY

American Petrographic Service, Inc. Report of Chloride-Ion Content AASHTO-T260 Procedure C. O'Fallon, IL: American Petrographic Service Inc, 2008.

American Traffic Safety Service Association (ATSSA). Structurally Deficient Bridges on the National Highway System. U.S. Department of Transportation Research and Innovative Technology Administration Bureau of Transportation Statistics Geospatial Information Program. October 22, 2008 <http://www.atssa.com/galleries/default-file/US_BridgeMap.pdf>.

Baker, G. S., Jordan, T. and Pardy, J. Introduction to Ground Penetrating Radar (GPR). Stratigraphic Analyses Using GPR. Ed. Gregory Baker and Harry Jol. Boulder, Colorado: Geological Society of America, 2007. 1-18.

Brown, R.P., Kessler R.J. and Florida department of Transportation. Fundamentals of Corrosion. Bridge Decks: Corrosion, Cathodic Protection, and Pavement Seals, (TRB) Record 604. Washington, D.C: Transportation Research Board, 1976. 16-19.

Cardimona, S., Willeford, B., Wenzlick, J. and Anderson, N. Bridge Decks Condition Studies in Missouri Utilizing Ground Penetrating Radar: RDT 01-012, Jefferson City, MO: MoDot, 2001.

Clemeña, G.G. and Apusen, C.M. An Alternative Potentiometric Method for Determining Chloride Content in Concrete Samples from Reinforced Concrete Bridges. Charlottesville, Virginia, 2002 <ttp://www.virginiadot.org/vtrc/main/online_reports/pdf/02-r18.pdf>.

Costley, R.D. Acoustic Testing of Concrete Bridge Decks. Gongkang Fu, ed. Inspection and Monitoring Techniques for Bridge and Civil Structures. Cambridge, England: Woodhead Publishing Ltd, 2005. 64-81.

Costley, R.D. Finding Delaminations in Concrete Bridge Decks. 146th Acoustical Society of America (ASA) Meeting. Austin, TX, 2005. September 22, 2008 <http://www.acoustics.org/press/146th/Costley.htm>.

Daniels, D.J., Ground Penetrating Radar (Iee Radar, Sonar, Navigation and Avionics Series). Stevenage, UK: Institution of Electrical Engineers, 2004.

---. Surface-Penetrating Radar (IEE Radar, Sonar, Navigation and Avionics Series, 6) Stevenage, UK: Institution of Electrical Engineers, 1996.

Federal Highway Administration (FHWA). 2007 National Bridge Inventory (NBI). October 15, 2008 <http://www.fhwa.dot.gov/bridge/structyr.htm>.

Federal Highway Administration (FHWA). Design of Continuously Reinforced Concrete Pavements Using Glass Fiber Reinforced Polymer Rebars. 2006, December 17, 2008 < http://www.fhwa.dot.gov/pavement/pccp/pubs/05081/chapt2.cfm>

Fromm, H.J., Wilson G.P. and Ontario Ministry of Transportation and Communications. Cathodic Protection of Bridge Decks: A Study of Three Ontario Bridges. Bridge Decks: Corrosion, Cathodic Protection, and Pavement Seals, (TRB) Record 604. Washington, D.C: Transportation Research Board, 1976. 38-47.

Geophysical Survey Systems, Inc. Bridge Assessment Module: RADAN 6.5 Users Manual MN 43-172 Rev C. Salem, New Hampshire: Geophysical System Survey Inc, 2007.

---. GSSI Handbook for Radar Inspection of Concrete: Manual MN72-367 Rev D. New Hampshire: Geophysical System Survey Inc, 2006.

---. GSSI SIR-3000 Users Manual. Salem, New Hampshire: Geophysical System Survey Inc 2006.

---. GSSI Handbook for Radar Inspection of Concrete GSSI Manual # MN72-367 Rev. D. New Hampshire: Geophysical System Survey Inc, 2005.

---. Operation Manual SIR System-2: GSSI Manual # MN72-140A. New Hampshire: Geophysical System Survey Inc, 1996.

Geophysical Survey System Inc (GSSI). Products. November 1,2008 <http://www.geophysical.com/products.htm>.

Guthrie, S. and Hema, J. Concrete Bridge Deck Condition Assessment Guidelines. Brigham Young University, Department of Civil & Environmental Engineering 2005. November 5, 2008 <http://www.udot.utah.gov/main/uconowner.gf?n=200505271053301>.

Iowa Department of Transportation. Bridge Inspection Definitions. October 17, 2008 <http://www.iowadot.gov/subcommittee/bridgetermspz.aspx#s>.

Jensen, V. Alkali-silica Reaction (ASR) Testing of Deterioration in Concrete. Gongkang Fu, ed. Inspection and Monitoring Techniques for Bridge and Civil Structures. Cambridge, England: Woodhead Publishing Ltd, 2005. 22-63.

Jestings, W.J., and Mahir, S. Bridge Engineering. Roger, Brockenbrough and Kenneth Boedecker Chapter 4, Brockenbrough and Boedecker, eds. Highway Engineering Handbook: Building and Rehabilitating the Infrastructure. 2nd Ed. New York: McGraw-Hill Companies Inc, 2003. Chapter 4.

Kim, W. Ground Penetrating Radar Application for Non-Destructive Testing: Bridge Deck Inspection and Dowel Bar Detection. Diss. Missouri University of Science and Technology formally University of Missouri Rolla, 2003.

Krauss, P.D., and Rogalla E.A. TransverseCracking in Newly Constructed Decks. Report 380, NationalCooperative Highway Research Program, 1996.

Lorrain, P., and Carson D.R. Electromagnetic Fields and Waves. 2nd ed. New York: W.H. Freeman and Company NY, 1970.

Lucius, J.E. and Powers, M.H. Multifrequency GPR Survey. Symposium on the Application of Geophysics to Engineering and Environmental Problems. Reno, NV: The Environmental and Engineering Society, 1997.

Maierhofer, C. "Nondestructive Evaluation of Concrete Infrustructure With Ground Penetrating Radar." Journal of Materials in Civil Engineering Volume 15, No.3 (2003): 287-297. October 1, 2008 <www.asce.org>.

Morse, A.A., and Roger L.G. Pavement Design and rehabilitation. Roger, Brockenbrough and Kenneth Boedecker, eds. Highway Engineering Handbook: Building and Rehabilitating the Infrastructure. 2nd Ed. New York: McGraw-Hill Companies Inc, 2003. Chapter 3.

Purdue University News. Purdue engineers study corrosion-resistant material for bridges. 2005. October 9, 2008 <http://news.uns.purdue.edu/html4ever/2005/051208.Frosch.bridges.html>.

Qian, S. Testing Steel Corrosion in Reinforced Concrete. Gongkang Fu, ed. Inspection and Monitoring Techniques for Bridge and Civil Structures. Cambridge, England: Woodhead Publishing Ltd, 2005. 1-18.

Reynolds, J.M. An Introduction to Applied and Environmental Geophysics. West Sussex, England: John Wiley & Sons Ltd, 1997.

Roberge, P.R. Corrosion Inspection and Monitoring. Hoboken, New Jersey: John Wiley & Sons Inc, 2007.

Sastri, V.S. Corrosion Inhibitors: Principles and Applications. West Sussex, England: John Wiley & Sons Ltd, 1998.

Sheriff, R.E. Encyclopedia Dictionary of Exploration Geophysics 2rd ed. Tulsa, OK: Society of Exploration Geophysicists, 1998.

Sohanghpurwala, A.A. Manual on Service Life of Corrosion-Damaged Reinforced Concrete Bridge Superstructure Elements. Washington, DC: Transportation Research Board, 2006. Report 558.

South Dakota Department of Transportation. August 2006. Feasibility of Using Ground Penetrating Radar (GPR) for Pavements, Utilities, and Bridges. October 1, 2008 <http://www.state.sd.us/Applications/HR19ResearchProjects/Projects%5CSD2005-05_Final_Report.pdf>.

Transportation Research Board (TRB). Durability of Concrete Bridge decks. National Cooperative Highway Research Program Synthesis of Highway Practice. Washington, DC: Transportation Research Board, 1976. Report 57.

Vector Corrosion Technologies. Standard Specification for Electrochemical Chloride Extraction: AASHTO Designation. November 1, 2008 < http://www.vector-corrosion.com/pdf/SEC_0009/DOC_0002.PDF>.

Webb, D.J. Ground Penetrating Radar: A Tool to Evaluate Bridge Scour. Thesis. Missouri University of Science and Technology formally University of Missouri – Rolla, 2000.

Yehia, S., Abudayyeh, O., Nabulsi, S. and Abdelqader, I. "Detection of Common Defects in Concrete Bridge Decks Using Nondestructive Evaluation Techniques." Journal of Bridge Engineering Volume 12, No.2 (2007): 215-225. 1 Oct. 2008 <www.asce.org>.

VITA

Amos Wamweya was born on November 23, 1980, in Molo, Rift Valley Province, Kenya. He received his primary school education in both St Mary's Boys Primary and Moto Primary School, in Molo, Kenya. In 1999, he graduated from Njoro Boys High School, in Njoro, Kenya. Mr. Wamweya began his collegiate studies in 2001 and received a Bachelor of Science Degree in Geology in 2005 from College of Charleston (CofC) in South Carolina. During his time at CofC Mr. Wamweya worked as a Teacher Assistant and was also involved in geochemistry, remote sensing research projects.

In 2007, Mr. Wamweya joined Missouri University of Science and Technology (MS&T) formally University of Missouri-Rolla (UMR) for a Masters Degree in Geological Engineering with an emphasis in Geophysics.

During his time in MS&T Mr Wamweya worked in various projects with different geophysical techniques including: resistivity, conductivity, magnetics, elecromagnetics, and seismic. He also worked as a Teaching Assistant in the application of the above name geophysical techniques and introductory geology lab. Mr Wamweya co-authored two papers which were published by the American Society of Civil Engineers (ASCE) during his two year stint at MS&T.